

# Variation of Solar Wind Parameters and Total Electron Content from Indian, Australian, Brazilian and South African Sectors during the Intense Geomagnetic Storms

Binod ADHIKARI<sup>1</sup>, Roshan Kumar Mishra<sup>2</sup>, Narayan P. Chapagain<sup>3</sup>, Rabin Baral<sup>2</sup>, Priyanka Kumari Das<sup>4</sup>, Virginia Klausner<sup>5</sup>, and Manisha Sharma<sup>2</sup>

<sup>1</sup>St.Xavier's College, ,Maitighar, Kathmandu, Nepal

<sup>2</sup>St. Xavier's College

<sup>3</sup>University of Illinois at Urbana Champaign

<sup>4</sup>St, Xavier's College

<sup>5</sup>Vale do Paraiba University

November 24, 2022

## Abstract

In this paper, we present the variations of IMF-Bz, Solar wind Parameters ( $V_{sw}$ ,  $N_{sw}$ , and  $P_{sw}$ ), and Geomagnetic Indices (AE and SYM-H), and the variation of Vertical Total Electron Content (VTEC) using simultaneous VTEC data from 12 GPS-TEC stations over the Indian, Australian, Brazilian and South African regions. We describe contrast in Total Electron Content (TEC) throughout the globe using global ionospheric maps at regular 2-hour interval of UT during the three intense geomagnetic storms. Moreover, we observed that heavily TEC influenced areas were found to be transposing through equatorial plane starting from eastern sectors to the western sectors. Indian Ocean, Atlantic Ocean and South Pacific Ocean sectors were affected flowingly. Global Ionospheric Maps evince that Indian and Brazilian sectors were affected heavily explaining the TID and Equatorial Anomaly as seen on those areas. The equatorial and low-latitude regions have been mainly affected by the geomagnetic storms. All these results suggested that the acute disruption of global winds (surging towards the equator from higher latitudes) and electric fields commenced from magnetosphere-ionosphere interaction cause the severe modification in the equatorial, low-latitude region. We checked the cross correlation during the period of high solar and geomagnetic activities; the correlation gradually increased with the near by stations by latitudes in most of the cases which was another intriguing result. the storms were affected globally which is why we believe that variation of TEC over various stations of the globe could turn out to be very helpful in predicting solar wind coupling with magnetosphere-ionosphere.

# Variation of Solar Wind Parameters and Total Electron Content from Indian, Australian, Brazilian and South African Sectors during the Intense Geomagnetic Storms

Roshan Kumar Mishra<sup>1</sup>, Binod Adhikari<sup>1,2\*</sup>, Narayan Prasad Chapagain<sup>3</sup>, Rabin Baral<sup>1</sup>, Priyanka Kumari Das<sup>1</sup>, Virginia Klausner<sup>4</sup>, Manisha Sharma<sup>1</sup>

<sup>1</sup>Department of Physics, St. Xavier's College, Tribhuvan University, Kathmandu, Nepal.

<sup>2</sup>Department of Physics, Patan Multiple College, Tribhuvan University, Nepal.

<sup>3</sup>Department of Physics, Amrit Science College, Tribhuvan University, Kathmandu, Nepal.

<sup>4</sup>Department of Physics, UNIVAP - Universidade do Vale do Paraíba

\*Corresponding Author: binod.adhi@gmail.com

## Abstract

Streams of the particle ejected from the sun and the extreme space weather conditions like storms, high-speed streamers (HSSs), interplanetary coronal mass ejections (ICMEs), corotating interaction regions (CIRs) and Interplanetary Shocks (IS) termed as geomagnetic storms have massive influence in the climate and component of the Earth's upper atmosphere such as total electron content (TEC). The Study of TEC helps to understand variation in ionospheric electron density during geomagnetic storms. Global Ionospheric Maps of TEC are a real-time mapping of GPS observations produced by ground-based stations. In this paper, we have analyzed three intense geomagnetic storms of the year 2015: during 16 - 21 March 2015 (The St. Patrick's Day storm), 21 - 24 June 2015 and 18 - 22 December 2015. We present the variations of IMF-Bz, Solar wind Parameters ( $V_{sw}$ ,  $N_{sw}$ , and  $P_{sw}$ ), and Geomagnetic Indices (AE and SYM-H), and the variation of Vertical Total Electron Content (VTEC) using simultaneous VTEC data from 12 GPS-TEC stations over the Indian, Australian, Brazilian and South African regions. We describe contrast in Total Electron Content (TEC) throughout the globe using global ionospheric maps at regular 2-hour interval of UT during the three intense geomagnetic storms. Moreover, we observed that heavily TEC influenced areas were found to be transposing through equatorial plane starting from eastern sectors to the western sectors. Indian Ocean, Atlantic Ocean and South Pacific Ocean sectors were affected flowingly. Global Ionospheric Maps evince that Indian and Brazilian sectors were affected heavily explaining the TID and Equatorial Anomaly as seen on those areas. The equatorial and low-latitude regions have been mainly affected by the geomagnetic storms. All these results suggested that the acute disruption of global winds (surging towards the equator from higher latitudes) and electric fields commenced from magnetosphere-ionosphere interaction cause the severe modification in the equatorial, low-latitude region. We also checked the cross correlation of *TEC* of LCK3 station and various other stations during the period of high solar and geomagnetic activities; the correlation gradually increased with the near by stations by latitudes in most of the cases which was another intriguing result. Thus this results suggested that the storms were affected globally which is why we believe

that variation of TEC over various stations of the globe could turn out to be very helpful in predicting solar wind coupling with magnetosphere-ionosphere.

**Keywords:** Geomagnetic Storm, Total Electron Content, Global Ionospheric map, Ionospheric storm

## 1. Introduction

Geomagnetic storm, a tangled process, is the result of the interaction of the highly boosted energetic solar wind with the Earth's magnetic field escorted by massive southward interplanetary magnetic field (IMF-Bz) component. The onset of a geomagnetic storm is characterized by abrupt inflation in the solar wind speed due to coronal mass ejections (CMEs), and by fabrication of intensified high-latitude ionospheric currents and convection abiding several hours (Astafyeva et al., 2015). Ionospheric response to solar activity is vital for satellite navigation, radio communication, radar detection and other systems using ionospheric electromagnetic wave signals. The change or response of the ionosphere due to the change in the dynamic features coming from the sun is known as ionospheric storm (Thomas et al., 2016). Onset time of the storm, its intensity, duration, season, local time are important parameters causing effects on ionosphere due to storms (Blagoveshchenskii, 2013; Liu and Shen 2017). Negative ionospheric storm is the depletion of the ionospheric electron density during storm time whereas the positive storm is the increment in the ionospheric electron density (Fagundes et al., 2016). Positive storm is dominant during winter while negative storm in summer (Thomas et al., 2016). Positive ionospheric storms are due to amplification in the equatorward neutral winds rising from the auroral latitude energy penetration (Prolss, 1995). During the growth phase of the geomagnetic storm, the magnetospheric electric field becomes sharp and the particle precipitation patterns inflate turning out extreme. Moreover, the electrojet currents, the Joule heating, and particle heating rates enhance during this phase which leads to innovation of the electromagnetic configuration or the redistribution of plasma density and drift dynamics of the equatorial and low latitude ionosphere due to huge deposition of energy, momentum over the elevated latitude (Ramsingh et al., 2015). Joule heating leads to deviation in the propagation of the global winds towards the equator generating traveling atmospheric disturbances (TADs) (de Abreu et al., 2014). Traveling ionospheric disturbances arise on the interaction of the ionosphere with the TADs (Killeen et al., 1984; Abreu et al., 2010, Duly et al., 2013).

The effect of the geomagnetic storm in the ionosphere-thermosphere region is the interesting and imperative matter in space weather events both for the practical goals and scientific fascination (Prolss, 1978; Sastri et al., 2000; Chapagain et al., 2013). The composition, density, circulation and dynamics of the ionosphere-thermosphere system are globally modified being the root of both escalating and slumping in TEC and electron plasma densities termed as positive and negative storms (Mendillo, 2006; Danilov, 2013; Astafyeva et al., 2015). The Study of TEC helps to understand variation in ionospheric electron density during geomagnetic storms. Numerous empirical, physical and semiempirical models (Anderson, 1973; Ezquer et al., 1992, 1994; Scida et al., 2016) are used for TEC evaluations and ionospheric conditions applied to

detect the position of satellite equivalent to radar-to-satellite path (Hartman and Leitinger, 1984) among which International Reference Ionosphere (IRI) is broadly used empirical model (Rawer et al., 1978; Bilitza and Reinisch, 2008). The IRI protracted to Plasmasphere (IRI Plas) (Gulyaeva et al., 2002) model portrays the exemplary conditions of solar and geomagnetic activities. Kikuchi et al. (1996, 2000) and Nishida (1968) devised the idea about turning of IMF-Bz towards southward due to the intensified convection electric field. IMF-Bz inclination towards south strengthens the current ionospheric zonal electric fields by PPEFs and PPEFs, makes the existing zonal electric fields weak during the northward turning, resulting most of the PPEFs effect due to variation of IMF-Bz (Nayak et al 2016). de Jesus et al. (2016) has studied the dynamics of the ionosphere and its response during the severe geomagnetic storm and observed exclusively specific features in solar cycle 24 in reference to other solar cycles. Simi et al. (2013) and Huang (2013) observed that acute disruption of global winds (surging towards the equator from higher latitudes) and electric fields commenced from magnetosphere-ionosphere interaction cause the severe modification in the equatorial, low-latitude region (de Abreu et al., 2014, Chapagain et al., 2012).

In this paper, we present and analyze the results using simultaneous VTEC data from 12 GPS-TEC stations over the Indian, Australian, Brazilian and South African regions during three different geomagnetic storms occurring declining phase of solar cycle 24. The first one is of 16 - 21 March 2015 (The St. Patrick's Day storm), the second one is of 21 - 24 June 2015 and the last one is of 18 - 22 December 2015.

## 2. Dataset

The data correspond to three intense geomagnetic storms of 2015. The first one is of 16 - 21 March 2015 (The St. Patrick's Day storm), the second one is of 21 - 24 June 2015 and the last one is of 18 - 22 December 2015. In this paper, we present and analyze the results using simultaneous VTEC data from 12 GPS-TEC stations over the Indian, Australian, Brazilian and South African regions. IMF-Bz, Solar wind parameters ( $V_{sw}$ ,  $N_{sw}$ ,  $P_{sw}$ ) and Geomagnetic indices (AE and SYM-H) data are obtained from the OMNI (<http://omniweb.gsfc.nasa.gov/form>) site. The RINEX Hatanaka compressed observation files extracted from the NASA website (<ftp://cddis.gsfc.nasa.gov/pub/gps/data>) are well processed by GOPI software, a GPS-TEC analysis application software (Seemala and Valladares, 2011). Ionex database derived from NASA site (<ftp://cddis.nasa.gov/pub/gps/products/ionex/>) are used to analyze and discuss the 2-hourly global ionospheric response maps. The conversion of geographical latitude and longitude to magnetic latitude and longitude was processed by World Data Center for Geomagnetism, Kyoto (<http://wdc.kugi.kyoto-u.ac.jp/igrf/gggm/>). The location, Symbols of stations considered, geographical and magnetic latitudes, geographical and magnetic longitudes, and conversion of local time and universal time in view of Daylight saving of the considered GPS stations is given in the tables below.

Table 1. The location, Symbols of stations considered, geographical and magnetic latitude, geographical and magnetic longitude, and conversion of local time and universal time in view of Daylight saving of the considered GPS stations

Indian Sector								
Location	Symbol Used	Geo Lat.	Geo Long	Mag Lat.	Mag Long.	Local Time (hrs) March	Local Time (hrs) June	Local Time (hrs) December
Hyderabad, India	HYDE00IND	17.42 °N	78.55 °E	8.77 °N	152.24 °E	UT + 5:30	UT + 5:30	UT + 5:30
Bangalore, India	IISC00IND	13.02 °N	77.57 °E	4.49 °N	150.93 °E	UT + 5:30	UT + 5:30	UT + 5:30
Lucknow, India	LCK300IND	26.91 °N	80.96 °E	18.01 °N	155.31 °E	UT + 5:30	UT + 5:30	UT + 5:30
Australian Sector								
Location	Symbol Used	Geo Lat.	Geo Long	Mag Lat.	Mag Long.	Local Time (hrs) March	Local Time (hrs) June	Local Time (hrs) December
Darwin, Australia	DARW00AUS	12.84 °S	131.13 °E	21.59 °S	155.00 °W	UT + 9:30	UT + 9:30	UT + 9:30
Mitchell, Australia	MCHL00AUS	26.36 °S	148.15 °E	33.34 °S	135.46 °W	UT + 10	UT + 10	UT + 10
Cape Ferguson, Australia	TOW200AUS	19.27 °S	147.06 °E	26.47 °S	137.64 °W	UT + 10	UT + 10	UT + 10
Brazilian Sector								
Location	Symbol Used	Geo Lat.	Geo Long	Mag Lat.	Mag Long.	Local Time (hrs) March	Local Time (hrs) June	Local Time (hrs) December
Brasilia, Brazil	BRAZ00BRA	15.95 S	47.88 °W	7.02 °S	23.94 °E	UT – 3	UT – 3	UT – 2
Salvador, Brazil	SAVO00BRA	12.94 S	38.43 °W	4.80 °S	33.35 °E	UT – 3	UT – 3	UT – 3
Curitiba, Brazil	UFPR00BRA	25.45 S	49.23 °W	16.36 °S	21.97 °E	UT - 3	UT - 3	UT - 2
South African Sector								
Location	Symbol Used	Geo Lat.	Geo Long	Mag Lat.	Mag Long.	Local Time (hrs) March	Local Time (hrs) June	Local Time (hrs) December
Krugersdorp, South Africa	HRAO00ZAF	25.89 °S	27.69 °E	27.08 °S	95.53 °E	UT + 2	UT + 2	UT + 2
Richardsbay, South Africa	RBAY00ZAF	28.80 °S	32.08 °E	30.66 °S	99.29 °E	UT + 2	UT + 2	UT + 2
Windhoek, Namibia	WIND00NAM	22.58 °S	17.09 °E	22.05 °S	85.74 °E	UT + 2	UT + 1	UT + 2



Fig. 1. Global map showing locations of the GPS receivers at different Indian, Australian, Brazilian and South African regions under IGS network.

### 3. Methodology

The cross-correlation measures the similarity between variables in time series and also explores unseen information [Katz, 1988, Liou et al., 2001; Adhikari *et al.*, 2017, 2018, and 2019,]. It is a measure of displacement of two series. The magnitude of this correlation coefficient varies between  $-1$  and  $+1$  (Katz, 1988). This method is regarded as a standardized procedure for measuring statistical relations among various parameters and for specifying a function of Time lead or lag (Adhikari *et al.*, 2018). In this research, it has applied to obtain correlation coefficients and time lag between TEC of Lucknow, India with others stations as mention on table 1. This analysis will help for determining the similarities as well as similar relative characteristics during geomagnetic storms (Katz, 1988).

### 4. Result and Discussion

#### Event\_1: 16 - 21 March 2015 (The St. Patrick's Day storm)

NOAA analysts briefed that Earth's magnetic field was hammered by bouncing blow of the cloud during the late hours of March 17<sup>th</sup> (Nava et al., 2016). Intense geomagnetic storm on 17<sup>th</sup> March (76 DOY) is the ramification of strike in the Earth's magnetosphere by partial halo coronal mass ejection (CME) derived from magnetic filament explosion from the sunspot

(Verkhoglyadova et al., 2016; Nayak et al., 2016) at 04:49 UT and has been called St. Patrick's Day geomagnetic storm. This geomagnetic storm is considered as the strongest geomagnetic storm of solar cycle 24. Instantaneous increase in flow speed, interplanetary magnetic field (IMF-B<sub>z</sub>) and solar wind pressure signifies the occurrence of CME (Verkhoglyadova et al., 2016). Resultant magnetic reconnection and southward components of the Alfvén waves are the incentive factors for the occurrence of geomagnetic activity (Verkhoglyadova et al., 2016).

Figure 2 exhibits the variations of IMF-B<sub>z</sub>, Solar wind Parameters (V<sub>sw</sub>, N<sub>sw</sub>, and P<sub>sw</sub>), and Geomagnetic Indices (AE and SYM-H) during the period of time from 16<sup>th</sup> to 21<sup>st</sup> March 2015, few days before the equinox. During the 16<sup>th</sup> March, IMF-B<sub>z</sub> turned northward with the highest magnitude of ~12 nT indicating weak magnetic activity. Solar wind speed increased progressively from ~300 km/s to ~440 km/s after dusk whereas, solar wind dynamic pressure is less than ~ 12.60 nPa. Arrival of interplanetary shock in the magnetosphere was stipulated by an unexpected increment in solar wind speed from ~401 km/s to ~504 km/s along with a sharp increase in solar wind dynamic pressure ~3 nPa to ~7nPa at ~ 04: 49 UT on 17<sup>th</sup> March 2015. Solar wind dynamic pressure was the reason for sudden storm commencement as marked by the increase in SYM-H (~67 nT) (Liu et al 2016). Onset of the sudden storm can be examined in the symmetrical ring current index (Sym-H). IMF B<sub>z</sub> was fluctuating sharply between North and South direction at the starting of 17<sup>th</sup> March till IMF-B<sub>z</sub> attained the highest value of 27.38 nT at 05:20 UT towards North, followed by sharp declination towards South at 06:18 UT with ~ -21.98nT. At 06:18 UT, augmentation of AE index started from ~356 nT, solar wind speed elevated to ~514 km/s specifying the magnetopause shock, solar wind density prolonged to ~22.77 n/cc, solar wind pressure to ~12.07 nPa and Sym-H to ~46 nT. IMF-B<sub>z</sub> steadily went back towards the north at 11:41 UT (19.16 nT) and abruptly turned towards South at 13:07 UT (-25.98nT). At 13:38 UT, IMF-B<sub>z</sub> sharply increased to 13.79 nT inclining towards North. After 13:48 UT, IMF-B<sub>z</sub> inclined towards south direction for an enduring time throughout the main phase except for minutes from 19:02 to 19:06 achieving the highest value of 11.06 nT at 19:05 UT. Rotation of IMF-B<sub>z</sub> towards northward direction initiates storm recovery. With the onset of recovery phase, IMF-B<sub>z</sub> starts to incline North and its values fluctuated in between (~ -10 to 10 nT) for the remaining of recovery period.

Significant increment of V<sub>sw</sub> is observed during 17<sup>th</sup> of March which ranged from (400-643) km/s. Average variation of solar wind speed was found to be ~550–600 km/s during the period of storm (Ramsingh et al., 2015). Solar wind speed was found comparatively large during the recovery phase ranging as much as 726 km/s. Solar wind density (N<sub>sw</sub>) and solar wind pressure (P<sub>sw</sub>) exhibits an analogous behavior throughout the storm time irrespective of minute difference in their magnitude. AE index procured the maximal value of 2298 nT at 13:58 UT on 17<sup>th</sup> March. The value of AE index fluctuates heavily until the end of main phase. There is no instantaneous substorm caused during this event, with reference to the AE index (Verkhoglyadova et al 2016). The SYM-H index extended to its maximum value of +67nT on 17<sup>th</sup> March at 04:49 UT (Storm Sudden Commencement, SSC) and minimum value was observed – 234 nT on 17<sup>th</sup> March at 22:47 UT, indicating the strongest storm of the solar cycle 24. Three phases (initial phase, main phase, and recovery phase) of this geomagnetic storm can be examined as 04:49 UT (Storm

Sudden Commencement, SSC) to 06:52 UT on 17th March as initial phase, 06:52 UT - 22:47 UT on 17<sup>th</sup> March as main phase and 22:47 UT on 17<sup>th</sup> March onwards as recovery phase.

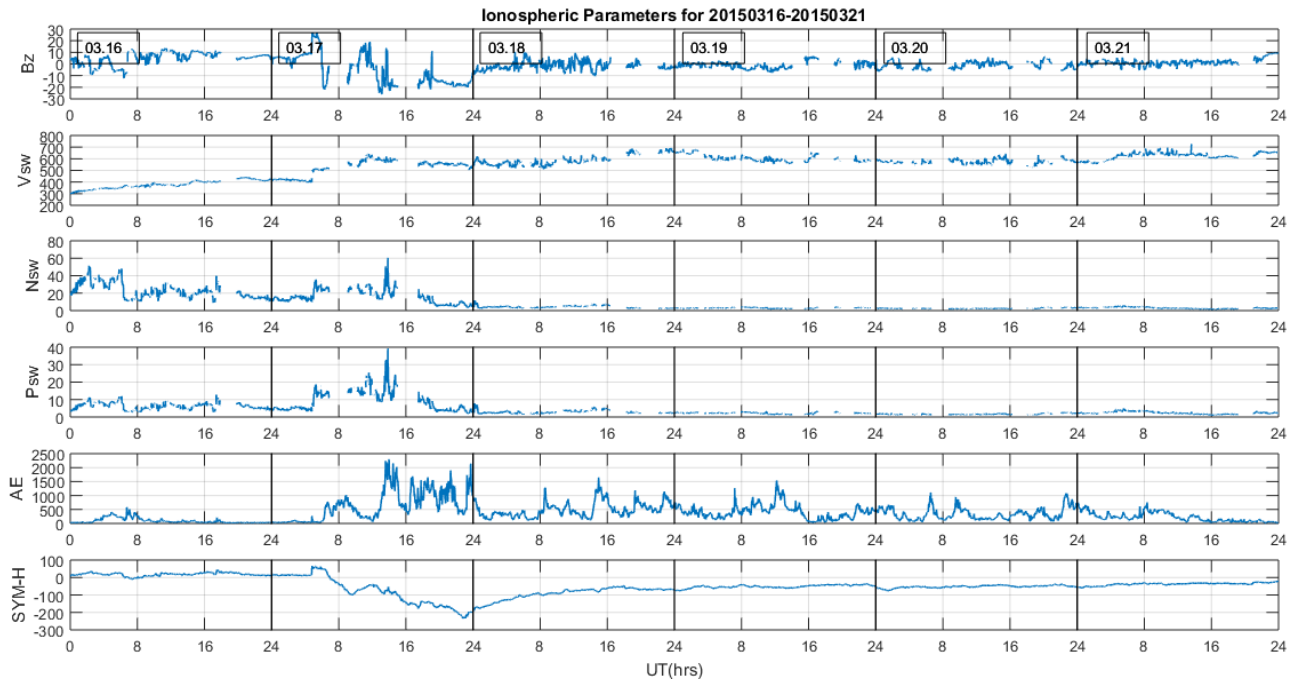


**Fig. 2.** z-component of interplanetary magnetic field IMF-Bz (nT), solar wind speed Vsw (km/s), solar wind density Nsw (cm<sup>3</sup>), solar wind pressure Psw (nPa), auroral electrojet AE index (nT) and symmetrical ring current index Sym-H (nT) for the period 16 March – 21 March 2015 are presented from top to bottom panels.

Figure 3 exemplifies the fluctuation of Vertical Total Electron Content (VTEC) of the storm with symmetrical ring current index Sym-H (nT) in an orderly interval of local time (hrs) during 16<sup>th</sup> of March to 21<sup>st</sup> of March 2015. VTEC observation from GPS Satellites in multiple stations of India, Australia, Brazil and Southern sectors of Africa are analyzed along with mean quiet day patterns (denoted by purple curve), calculated using the data for the five quietest days of the month. VTEC variations observed in iisc, hyde, lck3 of India comprising mostly low latitudinal regions is demonstrated on second panel of the graph. Increment of VTEC values can be seen as day starts, reaching maximum before dusk then decreases as the day comes to end. Wave-like pattern can be observed on each day (16<sup>th</sup> – 21<sup>st</sup> March) without any strong relatedness with other solar and geomagnetic parameters. Since 17<sup>th</sup> March portrays the main phase of St. Patrick’s Day storm, there are no significant reasons to interlink the variation of VTEC with the main phase of the storm. VTEC variation observed at iisc and hyde exhibits a regular pattern of fluctuation throughout the storm days ranging from 40-80 TECU. Whereas the Indian station lck3 exhibits a different pattern with the minimum value of VTEC at the initial recovery day

(18<sup>th</sup> March) and a high value of VTEC on the pre-storm day (16<sup>th</sup> March), and recovery days 20<sup>th</sup> and 21<sup>st</sup> March. 16<sup>th</sup> March exhibits quiet time variation and reduction of VTEC due to fountain effect after the day time in all the stations (Ramsingh et al., 2015). On 17<sup>th</sup> March after SCC at 4:49 UT, VTEC started to show a sudden increase in its value in all the stations. These enhancements are analogous with respect to time, caused by electric field – driven variation, which happens during main phase (Ramsingh et al., 2015). Negative storm effect is observed earlier in the Asian sectors than other regions (Nava et al., 2016). Maximum impact of negative phase is seen in the Asian sector and is related to large inputs of energy during evening and night period (Nava et al., 2016). Third panel of the graph explains the variation of VTEC in Australian sector consisting of darw, tow2 and mchl lower latitudinal stations. At the beginning VTEC values fluctuations are analogous to quiet day curve, before exhibiting wave like structure except on 18<sup>th</sup> March. All three stations experience a minimum VTEC count on the initial recovery day (18<sup>th</sup> March).

Fourth panel of the graph depicts the fluctuation of VTEC in low latitudinal (braz, savo and ufpr) stations of Brazil. VTEC plots represented by the graph specifies low-latitude stations are severely influenced by the geomagnetic storms stipulating three positive ionospheric storm peaks during the main phase at ~13:50 LT, ~17:55 LT and ~20:58 LT on 17<sup>th</sup> of March 2015. Three positive ionospheric storm peaks at the same time interval specify the disappearance of wave propagation characteristics (Fagundes et al., 2016) and VTEC values are generally lower than average quiet day of the month. During the main phase, positive ionospheric storm effect showed unusual characteristics of peaks resulting to increase and decrease in the VTEC. Increase and decrease in VTEC exhibit wavelike features (Tidal Ionospheric Disturbances: TID) especially at low latitudes. TID are initiated at high latitudes and travel towards the equatorial direction (de Abreu et al., 2010a; Lima et al., 2004). The wavelike oscillations are the cause of prompt penetration of electric field (PPEF) rather by the TIDs (Fagundes et al., 2016). VTEC variations indicate the positive and mighty ionospheric storm peaks in the Brazilian west sectors than those of East for low- latitudinal regions. Negative ionospheric storm (NIS) is observed during the recovery phase over the Brazilian regions (Fagundes et al., 2016).

VTEC variation in the South African region comprises of hrao, rbay and wind stations. At the start VTEC values are seen small and inseparable from mean quiet day but gradually it attains maximum value during midday and decreases gradually. Declination of VTEC marks the occurrence of negative storm (Verkhoglyadova et al., 2016). There is no proper correlation between SYM-H values and fluctuation of VTEC. Negative storm was marked during evenings with reference to TEC in both mid and low latitudinal sectors (Verkhoglyadova et al., 2016). During morning period of the day, low - latitudinal VTEC data has no significant relation to geomagnetic activity throughout the geomagnetic storm (Ramsingh et al., 2015, Verkhoglyadova et al., 2016). Positive storm effects observed in the figure are associated with different energy inserts as represented by AE magnetic index (Verkhoglyadova et al., 2016, Fagundes et al., 2016).

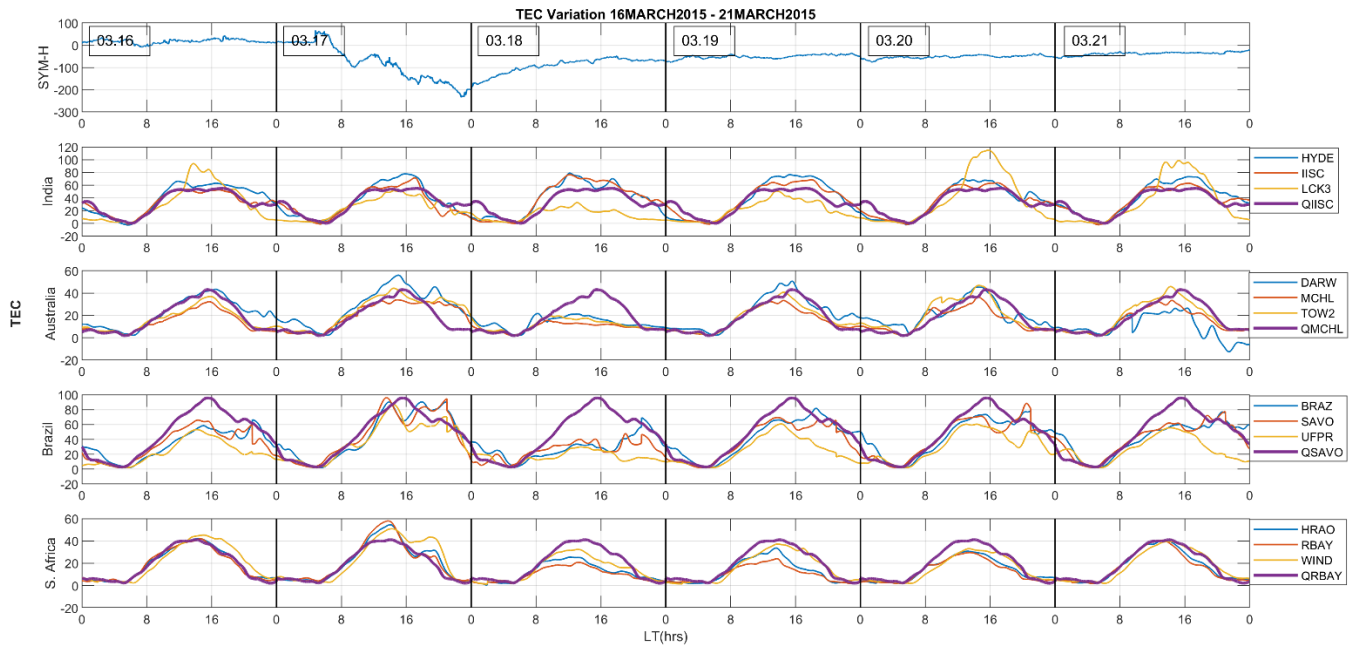


Fig. 3. VTEC variation observed on multiple stations of India (hyde, iisc, lck3), Australia (darw, mchl, tow2) Brazil (braz, savo, ufpr) and South Africa (hrao, rbay, wind) from 16th of March to 21st of March 2015 at regular intervals of LT are presented from top to bottom panels along with the mean quiet day.

Figures 4 and 5 describe contrast in TEC throughout the globe at a regular 2-hour interval of UT during the geomagnetic storm of 17<sup>th</sup> and 18<sup>th</sup> March 2015. Contour along with color gradient reflects global TEC intensity. For evaluation of changes in ionosphere developed by storms, high to low TEC activity ratio can be compared at any spatiotemporal location. Figures unveil ionospheric maps as a function of geographic longitude and latitude over a global map, attained using various GPS-TPS stations situated at India, Australia, Brazil, and South Africa. Global contour plot exhibits the alteration in TEC with the difference of 2 hours starting from 00:00 UT. The equatorial region is where the highest spatial and temporal value variations of the TEC are realized and where various features of the ionosphere, such as the equatorial anomaly and scintillation can be found (Paulo de Oliveira, 2009). So, our main focus is in the band of 30 degrees north - 30 degrees south of earth's equator, mainly Brazilian, South African, Indian and Australian sectors.

At the start 00:00 UT on 17<sup>th</sup> March, the TEC appears to be marginally intensified over the Pacific Ocean with minimum TEC intensity over the Indian region as compared to Brazilian, South African, and Australian sectors below. At 02:00 UT, TEC concentration is further enhanced over the Pacific Ocean. Between 04:00 UT and 06:00 UT, strong activity is initiated over the Indian regions with mild increment over Australian sectors compared to South American and African sectors. Images from 06:00 UT to 08:00 UT parade a significant surge in electron content over southern China and Taiwan (> 100 TECU) and growing activity over India. The South African region shows a mild increase in TEC while the TEC at Brazilian sectors are

below 20 TECU. As time progresses, the TEC intensification shown by the yellow colored contour on the map, appears to be shifting westwards towards the South African region and Brazilian sectors. At 10:00 UT, there is an appropriate hike in TEC over Indian Ocean, Southern part of China and India ( $>100$  TECU). It is also observed that TEC is seemingly increasing over Eastern African regions. At 12:00 UT, Eastern African sectors are marked to have strong TEC along with India and Indian Ocean sectors. However, mild increment of TEC can be viewed over South American regions. At 14:00 UT, TEC starts to decline over Australia, India and Indian Ocean, shifting toward Eastern part of South America from the western parts of Africa through Southern Atlantic Ocean. As we approach 16:00 UT, TEC is robust (100-120 TECU) over central Africa, South Atlantic Ocean and Brazil. TEC starts shifting away from African regions towards the South American sectors at 18:00 UT. There is a strong indication of TEC over Atlantic Ocean and Northern part of South America along with significant lessening of TEC over Australian and Indian regions. From 20:00 UT - 22:00 UT, TEC remains strong over western part of South America along with Brazil and Pacific Ocean near the Southern American region.

17<sup>th</sup> March portrays the main phase of geomagnetic storm. As per our study, recovery phase initiates from extreme late hours of 17<sup>th</sup> March, Ionospheric map on early hours of 18<sup>th</sup> March i.e. 00:00 UT shows TEC values  $> 100$  TECU over Brazil, Colombia and associated Pacific Ocean. The Australian and African regions seem to have TEC values lesser than 60 TECU with minimum over Indian regions. Gradual decrease in TEC all over the low latitudinal regions after 02:00 UT is initiated on 18<sup>th</sup> March. This is suggestive to the fact that the main phase of storm was between 04:49 UT - 22:47 UT on 17<sup>th</sup> March followed by the recovery phase afterward. Presence of strong TEC is seen till 2:00 UT at Pacific Ocean along with North American sector on 18<sup>th</sup> March. From 04:00 UT - 06:00 UT, Indian sector exhibits significant increment of TEC whereas South America exhibits significant decrement in TEC. Gradual intensification of TEC is observed to be moving westward from 08:00 UT - 14:00 UT along the equatorial and lower latitudinal regions of African continent from Indian region ranging from 60-120 TECU. From 16:00UT-20:00 UT, intensification is reduced slightly and prolongs to equatorial region of South America. The end of 18<sup>th</sup> March is characterized by heightening of TEC past central Pacific Ocean. It is observed that the TEC shifting phenomena of lower latitudinal region proceeds from eastern sector to western sector throughout the globe. Occurrence of high TEC is observed during positive storm effect and low during the negative storm. Post sunset enhancement isn't observed during 18<sup>th</sup> March. TEC is seen vigorous near equatorial plane and heavy declination of TEC is seen at higher latitudes.

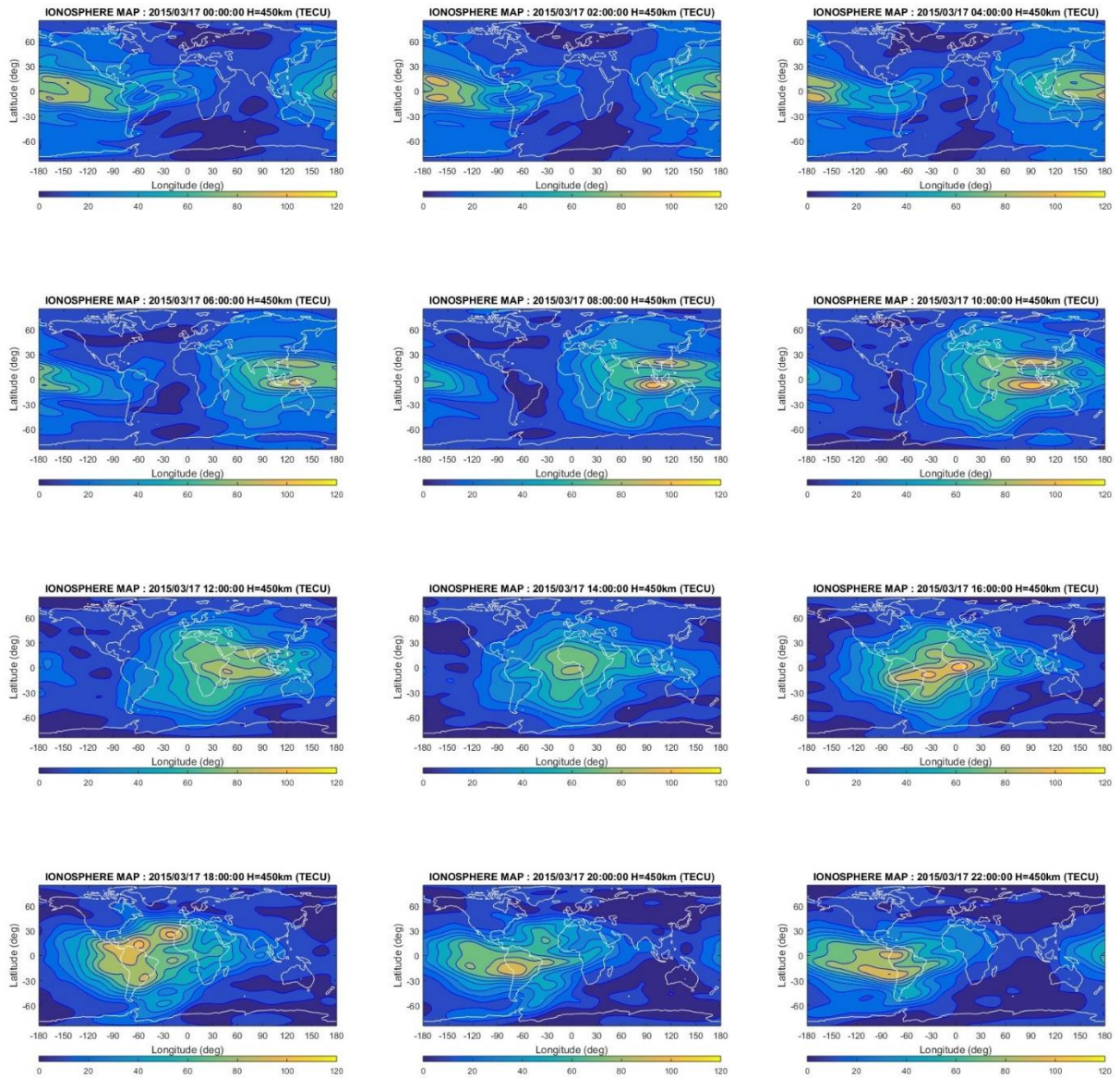


Fig. 4. Global GPS-TEC maps portraying geomagnetically disturbed days of 17th March 2015 at regular interval of 2 hours in UT.

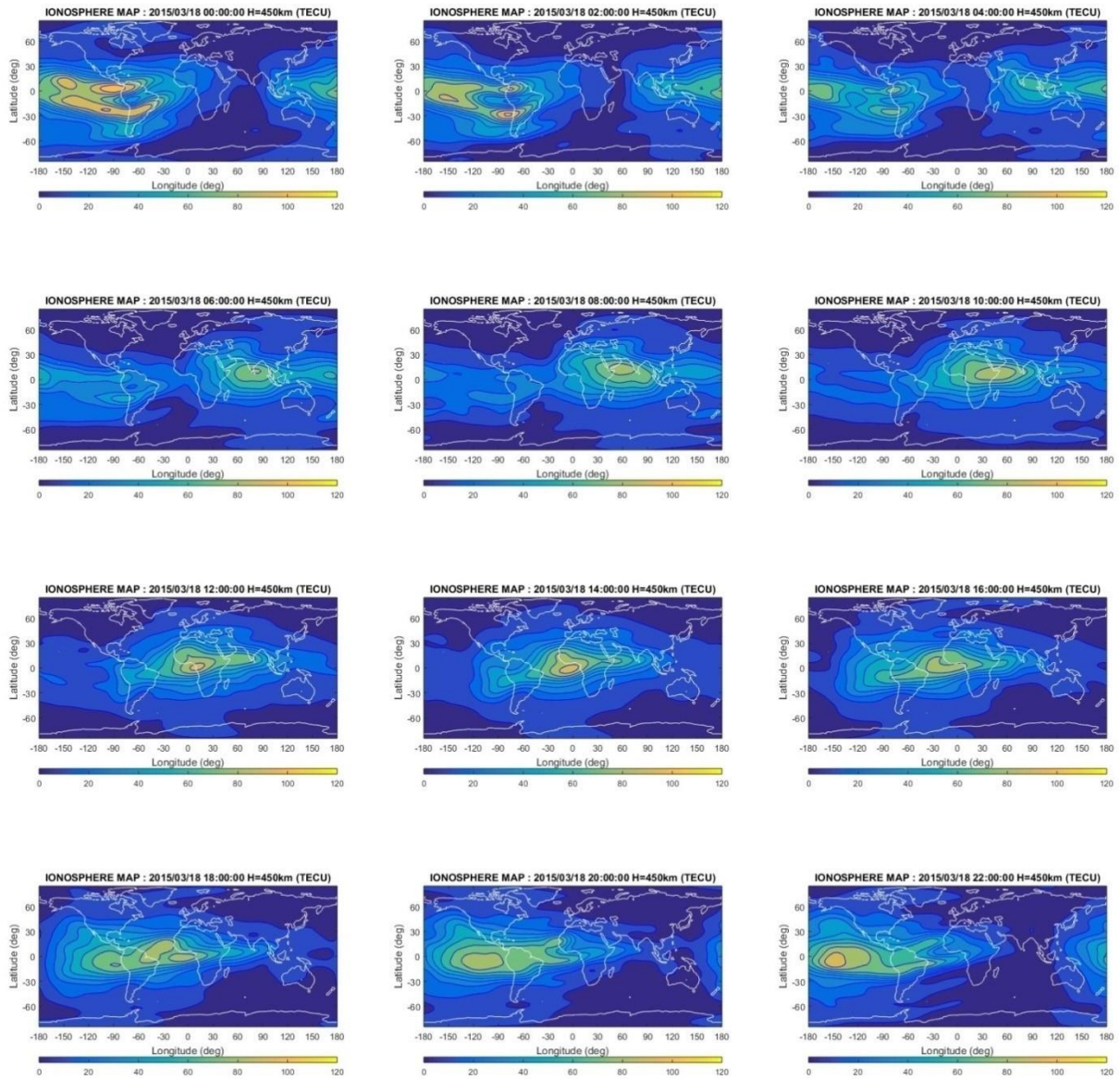
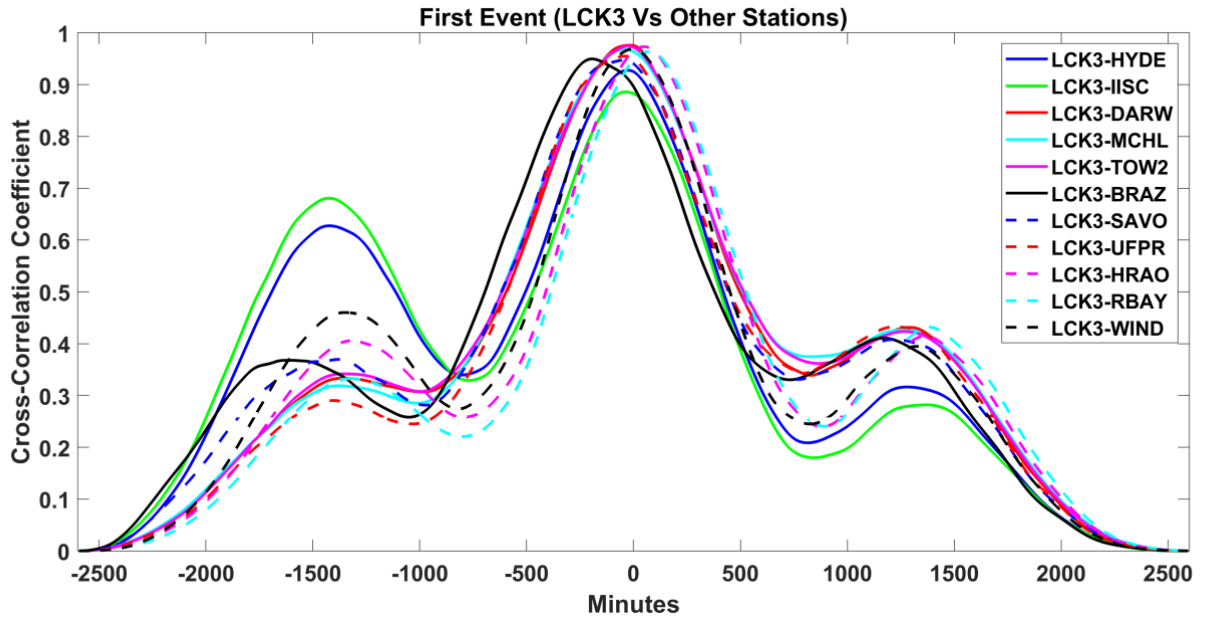


Fig. 5. Global GPS-TEC maps portraying geomagnetically disturbed days of 18th March 2015 at regular interval of 2 hours in UT.



**Figure 6.** Cross-correlation of symmetric horizontal component of geomagnetic field (SYM-H) of LCK3 station with other stations, HYDE (solid blue), IISC (solid green), DARW (solid red), MCHL (solid sky blue), TOW2 (solid pink), BRAZ (solid black), SAVO (dotted blue), UFPR (dotted red), HRAO (dotted pink), RBAY (dotted sky blue) and WIND (dotted black) during intense storm occurred on 17-18 March 2015.

Figure 6 depicts the results of cross correlation coefficient of *TEC* of LCK3 station (as a reference station, chosen randomly) in India with other stations of India, Australia, Brazil and South Africa during the intense storm occurred on 17-18 March 2015. The horizontal plane represents the time scale ranging from -2500 to 2500 min and the vertical plane represents the cross-correlation coefficient scale from 0 to 1. It is observed that station LCK3 correlates positively with other stations. LCK3-DARW (solid red), LCK3-MCHL (solid sky blue) and LCK3-TOW2 (solid pink) perfectly overlap with each other reaching the maximum positive correlation coefficient of 0.983 (approximately) at time lag -20 min. Since, they are strongly and positively correlated, they are said to be in phase [Adhikari et al., 2018]. Similarly, LCK3-HRAO (dotted pink) and LCK3-RBAY (dotted sky blue) reflects the highest positive correlation coefficient 0.978 where LCK3 leads HRAO and RBAY by 50 min. Moreover, LCK3-HYDE (solid blue) and LCK3-IISC (solid green) represents the strong positive correlation twice. In case of LCK3-HYDE curve, we can see the maximal positive cross correlation coefficient of 0.633 at -1440 min time lag and 0.935 at -20 min time lag. Meanwhile, LCK3-IISC reflects the strong positive correlation coefficient of 0.691 at -1430 min time lag and 0.889 at -20 min time lag. LCK3 positively correlates with other stations as well denoting in phase.

## Event\_2: 21 - 24 June 2015

Figure 7 exhibits the variations of IMF-Bz, Solar wind Parameters ( $V_{sw}$ ,  $N_{sw}$ , and  $P_{sw}$ ), and Geomagnetic Indices (AE and SYM-H) during the period of time from 21<sup>st</sup> to 24<sup>th</sup> June 2015, where the arrival of three Interplanetary Shocks (IS) is observed. These three IS of different intensities initiated from the Sun's active region 2371, were associated with coronal mass ejections (CMEs) (Liu et al., 2016). Initial arrival of two IS were observed at 16:52 UT on 21<sup>st</sup> June and 05:49 UT on 22<sup>nd</sup> June which were related with halo and partial-halo CME due to filament eruption on 18<sup>th</sup> and 19<sup>th</sup> June (Astafyeva et al., 2017). The third IS is humongous to the previous two, its arrival was observed at 18:37 UT on 22<sup>nd</sup> June and was associated with full halo giant CME (Astafyeva et al., 2017). Post the entrance of strong IS and CME, there was abrupt loss of energetic particles due to the huge increment of solar wind dynamic pressure (Baker et al., 2016). Figure manifests sudden changes in the solar wind speed, density and amplitude of the interplanetary magnetic field (IMF-Bz) during all three IS events. The AE index designates the magnetospheric energy displaced to the auroral oval and usually used as a substitute of Joule heating near the auroral arcs (Cherniak and Zakharenkova, 2017). Main causes of geomagnetic disturbances (substorms and storms) are southward-directed IMF-Bz component, that generates the recombination with the Earth's magnetic field lines. Beside IMF-Bz component, the solar wind speed and density plays key role in the might of an IS impact (Gonzalez et al., 1994).

During the advent of the first IS event the solar wind increases to 322 km/s, solar wind density sharply changes from 16 n/cc to 40 n/cc with flow pressure reaching up to 9.47 nPa. Due to these changes, there was sudden increment on SYM-H index ( $\sim 43$  nT). Positive IMF-Bz ( $\sim 1.05$  nT) and AE index ( $\sim 196$  nT) indicates there was no substorm (Astafyeva et al., 2017). Occurrence of second IS was indicated by increment in the solar wind speed ( $\sim 427$  km/s), change in SYM-H index from  $\sim 10$  nT – 38 nT, inclination of IMF-Bz towards South ( $-9.77$  nT) and increase in AE-index to 532. The appearance of the third IS was accompanied by a giant CME at 18:37 UT on 22<sup>nd</sup> June (Astafyeva et al., 2017). There was remarkable accretion in the solar wind speed ( $\sim 437$  km/s to 639 km/s), proton density from  $\sim 10$  n/cc to  $\sim 60$  n/cc and SYM-H index reaches to 88 nT. IMF-Bz component was strong and inclined towards south ( $-16.57$  nT) at the arrival. Considering the fluctuation of the SYM-H index, this is the second largest storm in the 24<sup>th</sup> solar cycle (Astafyeva et al., 2017). The June 2015 storm was specified by increased substorm activity. Main phase of the storm begins at 19:18 UT on 22<sup>nd</sup> June and AE index reaching up to 1476 nT. Analyzing the SYM-H value ( $-208$  nT) and AE index (1040 nT), recovery phase starts from  $\sim 04:28$  UT of 23<sup>rd</sup> June. Solar wind density ( $N_{sw}$ ) and solar wind pressure ( $P_{sw}$ ) exhibits an analogous behavior throughout the storm time irrespective of minute difference in their magnitude as in St. Patrick's Day storm.

The IMF-Bz has inclined southward from 18:38 UT to 19:47 UT on 22<sup>nd</sup> June with a minimum value  $-38.98$  nT at 19:23 UT.  $-38.98$  nT is the most negative inclination of IMF-Bz measured in 2015 (Cherniak and Zakharenkova 2017; Astafyeva et al., 2017). Value of IMF-Bz on 23<sup>rd</sup> June went through the numerous inclinations from south-north. At 01:57 UT, inclination was towards south and remained negative till 05:38 UT before inclination was observed towards north for a

couple of hours. One of the main traits of this storm is significant fluctuations of IMF-Bz during main phase and recovery phase (Astafyeva et al., 2017).

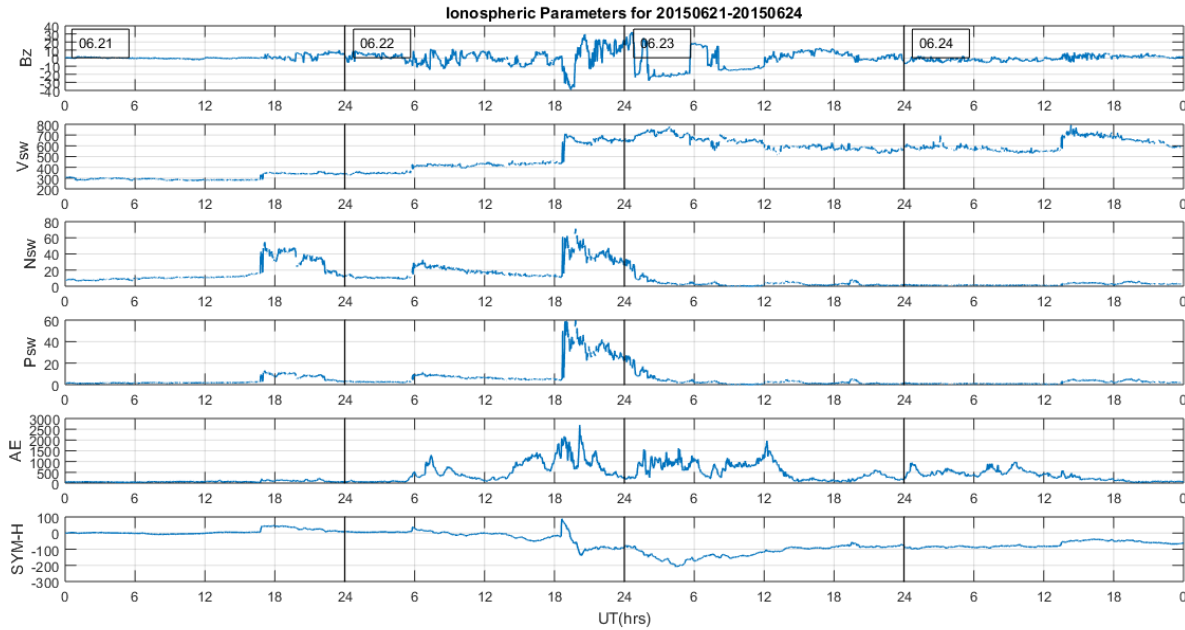


Fig. 7. z-component of interplanetary magnetic field IMF-Bz (nT), solar wind speed Vsw (km/s), solar wind density (cm<sup>3</sup>), solar wind pressure (nPa), auroral electrojet AE index (nT) and symmetrical ring current index Sym-H (nT) for the period 21 June – 24 June 2015 are presented from top to bottom panels

Figure 8 illustrates the fluctuation of VTEC at the previously mentioned stations over the duration of 21<sup>st</sup> June to 23<sup>rd</sup> June 2015 along with mean quiet day. As discussed initially, arrival of three IS were observed at 16:52 UT on 21<sup>st</sup> June, 05:49 UT and 18:37 UT on 22<sup>nd</sup> June with increment in SYM – H values (43 nT, 38 nT and 88 nT). During first IS, value of VTEC at Indian stations (hyde, iisc, lck3) were observed as 34.13 37.08 and 26,. At Australian stations (darw, mchl, tow2) VTEC values were recorded as 18.53, 12.29 and 13.73 respectively. At Brazilian stations (braz, savo, ufpr) values of VTEC was observed as (19.88, 15.27 & 12.93) and (9.51, 10.15 & 10.91) at S. African stations (hrao, rbay, wind). On second IS VTEC values for Indian, Australian, Brazilian and South African stations were observed as (7.45, 6.86, 13.19), (3.26, 2.75, 2.34), (2.93, 4.81, 3.36) and (4.13, 2.36, 4.28). Similarly, (25.9, 29.25, 23.63), (12.13, 7.14, 7.64), (32.53, 27.42, 10.8) and (8.07, 6.93, 8.93) at the third IS shock. Generally, Indian stations portray higher magnitude of VTEC during all three IS events as compared to other stations. Main phase of the storm begins at 19:18 UT on 22<sup>nd</sup> June and recovery phase starts from ~ 04:28 UT on 23<sup>rd</sup> June. During main phase, fluctuations of VTEC recorded at Indian, Australian, Brazilian and South African Region were (21.61, 24.51, 22.48), (10.15, 5.72, 6.2), (21.44, 18.36, 10.5) and (6.45, 5.9, 7.34). Similarly (2.06, 2.09, 2.09), (3.12, 4.41, 5.51), (3.72, 2.64, 3.78) and (5.14, 4.98, 4.46) at the starting of recovery phase. Main phase of the

storm exhibits negative storm whereas the recovery phase exhibits positive storm. Apart from 23<sup>rd</sup> June, VTEC values of respective stations aren't too deviated than the quiet day values .

During the pre-sunrise period small movement of VTEC could be seen. It begins to increase in day time. Storm enhance density are nearly linked with positive disturbances of daytime due to plasma upliftment directed perpendicular to magnetic field and eastward electric field (Takashi et. al., 2009). Positive phase of ionospheric storm is observed during day time (Blanc and Richmond, 1980). During daytime temperature increases along with the production rate of TEC. This results gradual increment in TEC from a morning minimum value to an afternoon maximum value. The primary source of ionization is no longer present in the evening where TECU remains minimal (Oryema et al., 2015). The electron content in the magnetic field collapse dramatically after the sunset on the response of less temperature in the thermosphere at the night time in equatorial and low latitudinal regions. Magnetic field gets filled rapidly just after the sunrise due to their low volume resulting in the steep increase in ionization. This TEC behavior might be the cause of production and loss rates of electrons in the ionosphere (Aggarwal, 2011).

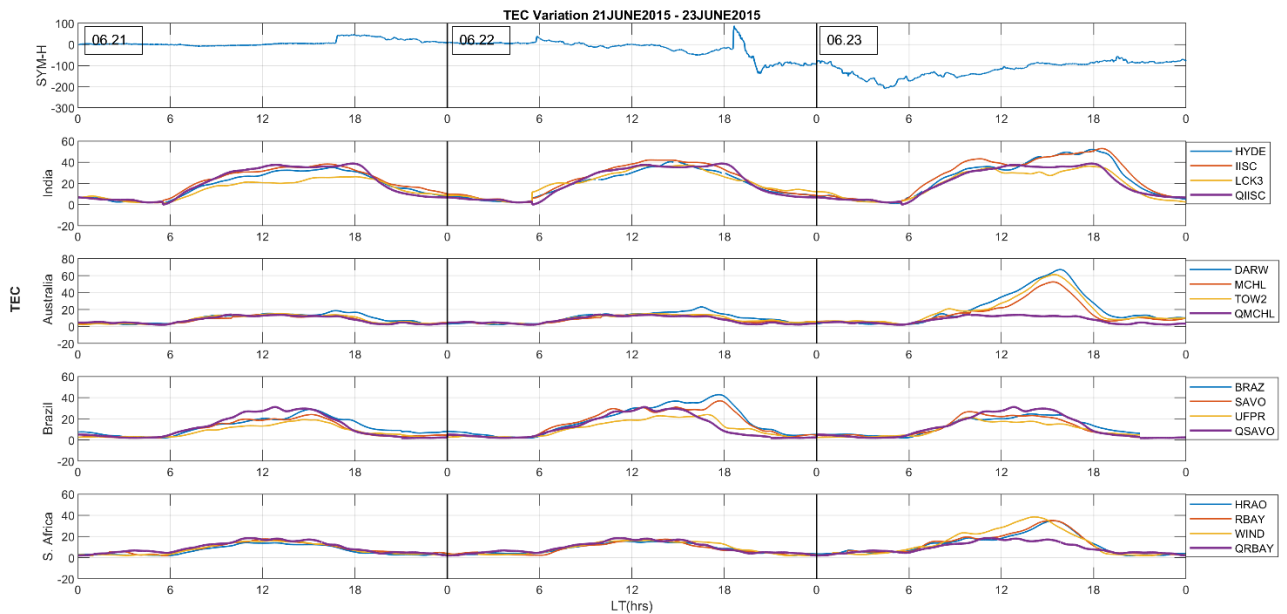


Fig. 8. VTEC variation observed on multiple stations of India (hyde, iisc, lck3), Australia (darw, mchl, tow2) Brazil (braz, savo, ufpr) and South Africa (hrao, rbay, wind) from 21st of June to 23 of June 2015 at regular intervals of LT are presented from top to bottom panels along with the mean quiet day

Figures 9 and 10 describe contrast in Total Electron Content (TEC) throughout the globe during the geomagnetic storm of 22<sup>nd</sup> and 23<sup>rd</sup> June 2015. At 00:00 UT, TEC content is strong over Pacific Ocean (40-60 TECU), relative to other parts of the map. From 02:00 UT – 04:00 UT mild intensification of TEC as seen initially prolongs towards lower latitudinal region (30 to -30 degree) of India and Australia. This mild TEC escalation elongates more towards Indian region and Northern China from 06:00-08:00 UT. At 08:00 UT, modest increment of TEC is seen at Eastern African region. At 10:00 UT, major concentration of TEC does situate at lower latitude (0 - 30° N) comprising Indian, Southern China, and Eastern African sectors. At 12:00 UT, TEC is maximum over Northern Africa. TEC concentration is observed to be shifting towards South American region via Northern Atlantic Ocean from Africa at 14:00 UT. From 16:00 UT – 18:00 UT, TEC is strong over Western and Central African regions along with South American regions and Pacific Ocean. From 20:00 UT- 22:00 UT, there is a comparative strong accumulation of TEC over Lower latitudinal North American regions, South America, North African regions, Atlantic and Pacific Ocean. Most intense TEC fluctuation of 22<sup>nd</sup> June is observed at 22:00 UT over lower latitudinal region of North America whereas after 18:00 UT, Indian and Australian sectors show minimum TEC concentration.

At 00:00 UT - 02:00 UT on 23<sup>rd</sup> March, TEC content is supplementary over northern Pacific and Atlantic Ocean. At 04:00 UT, TEC concentration initiates acceleration over Northern Australian sectors, Bay of Bengal, Indonesia and Malaysia and becomes intense at 06:00 UT. At this stage, Northern Australian sectors show significant TEC relative to others. From 08:00 UT - 10:00 UT, TEC concentration lessens than previous couple of hours at Bay of Bengal and Philippine Sea and mild intensification of TEC is seen over Indian region and Eastern Africa. At 12:00 UT, lower latitudinal regions of Africa and India evinces mild TEC over the region. This intensification lasts until 16:00 UT over central African regions and until 14:00 UT over Indian regions. After 16:00 UT, TEC concentration is remarkable low throughout the globe ranging 20-40 TECU, which prolongs through equatorial plane covering low latitudinal regions till the day finishes.

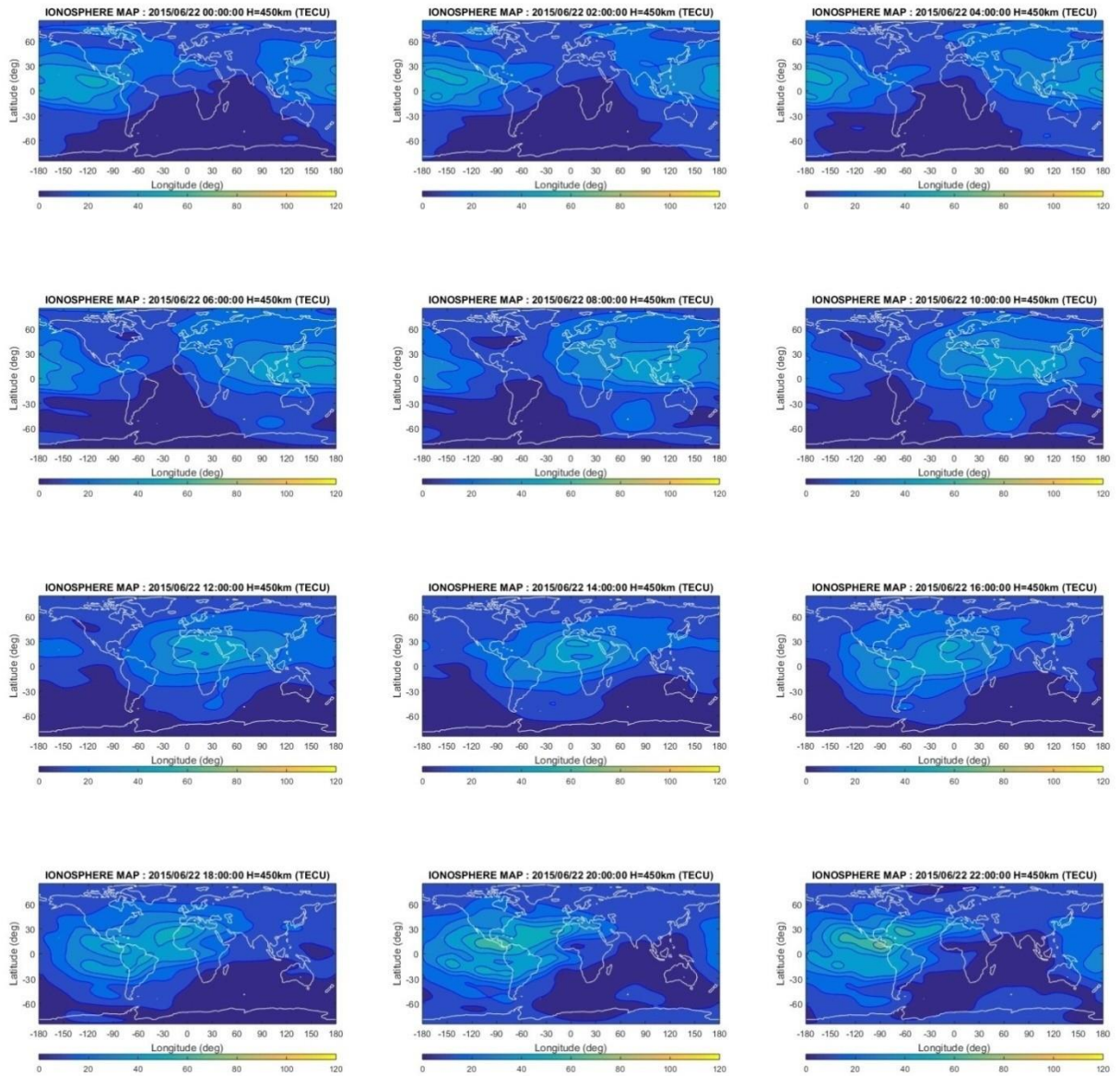


Fig. 9. Global GPS-TEC maps portraying geomagnetically disturbed days of 22nd June 2015 at regular interval of 2 hours in UT.

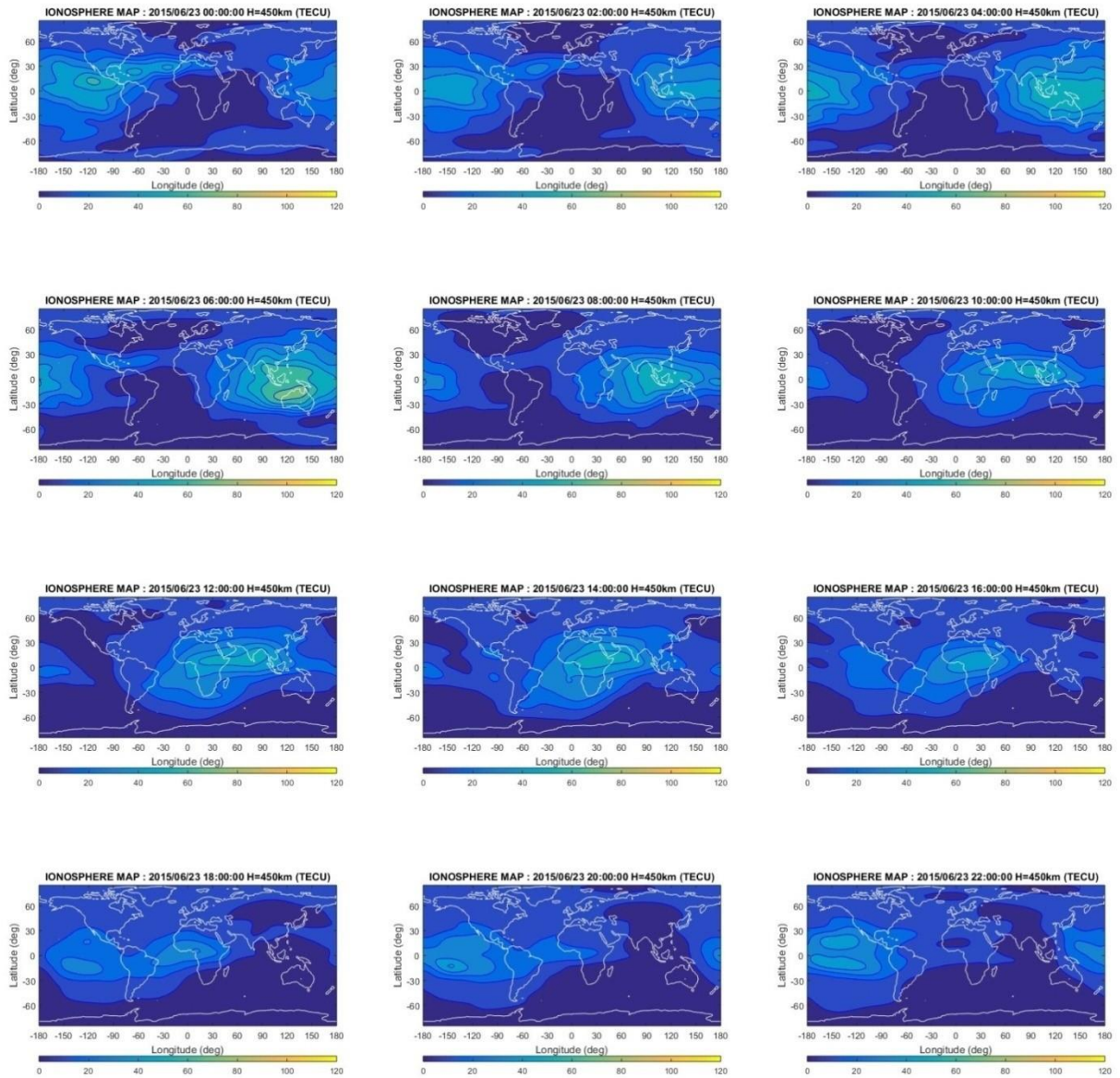
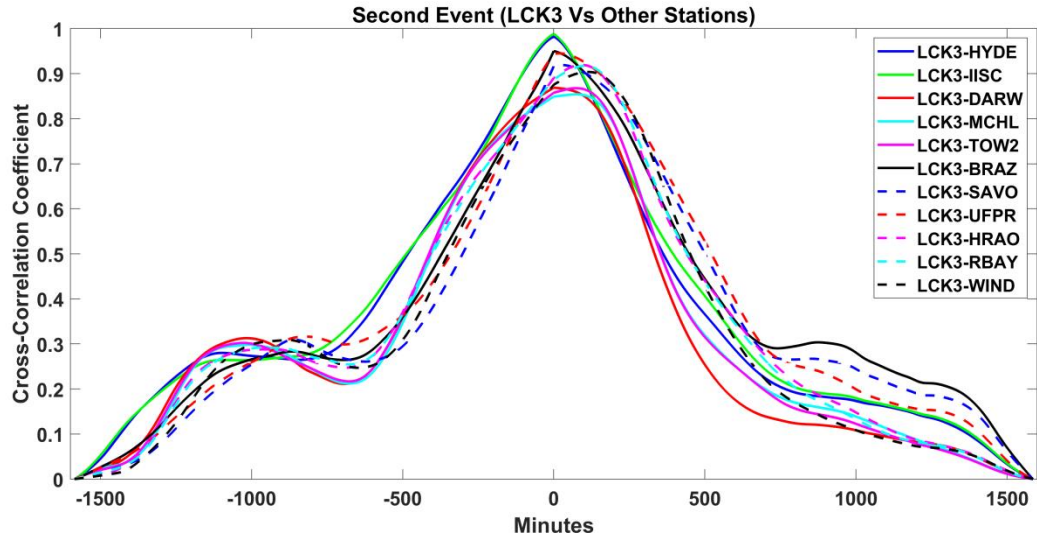


Fig. 10. Global GPS-TEC maps portraying geomagnetically disturbed days of 23rd June 2015 at regular interval of 2 hours in UT.



**Figure 11.** Cross-correlation of symmetric horizontal component of geomagnetic field (SYM-H) of LCK3 station with other stations, HYDE (solid blue), IISC (solid green), DARW (solid red), MCHL (solid sky blue), TOW2 (solid pink), BRAZ (solid black), SAVO (dotted blue), UFPR (dotted red), HRAO (dotted pink), RBAY (dotted sky blue) and WIND (dotted black) during intense storm occurred on 22-23 June 2015.

The cross-correlation coefficient versus time scale has been plotted in figure 11 during the event on 22-23 June 2015. The x-axis portrays time scale ranging from -1500 to 1500 min and the y-axis portrays the cross-correlation coefficient ranging from 0 to 1. Most of the plots show identical nature. LCK3-HYDE (solid blue) and LCK3-IISC (solid green) curve almost overlapped delineating the highest positive correlation coefficient of 0.991 at 0 min. This means that LCK3 and HYDE, LCK3 and IISC are in phase. Meanwhile, at the same time, LCK3-UFPR (dotted red) and LCK3-BRAZ (solid black) reveals the highest positive correlation coefficient of 0.963. Similarly, LCK3-HRAO (dotted pink) and LCK3-RBAY (dotted sky blue) curve shows the overlapping nature attaining the strong positive cross-correlation coefficient 0.927 where LCK3 leads HRAO and RBAY by 130 min. Furthermore, LCK3-MCHL (solid sky blue) and LCK3-TOW2 (solid pink) show the identical nature indicating the strong correlation coefficient of 0.872 and 0.882 respectively at which LCK3 leads MCHL and TOW2 by 100 min. Moreover, we can see the very good correlation coefficient between LCK3 and other stations ranging from 0.872 to 0.925 at time lead interval from 30 to 150 min.

### **Event 3: 19 - 22 December 2015**

Figure 12 depicts the variations of IMF-Bz, Solar wind Parameters ( $V_{sw}$ ,  $N_{sw}$ , and  $P_{sw}$ ), and Geomagnetic Indices (AE and SYM-H) during the period of time from 19<sup>th</sup> to 22<sup>nd</sup> December 2015. This event is explored as the imperative event in this paper having a peculiar nature. The onset of a massive geomagnetic storm or sudden storm commencement (SSC) was at ~16:18 UT on 19<sup>th</sup> December, characterized by the sudden compression of Earth's magnetosphere due to highly boosted energetic solar wind emanated from CMEs (Richardson and Cane, 2012) near the Winter Solstice of the year 2015. As a result, the thermal, chemical and electrodynamic stability

of solar-terrestrial space system gets disturbed inducing several irregularities in ionosphere, plasmasphere, thermosphere and magnetosphere (Jin et al., 2017). After the initiation of SSC, IMF-B<sub>Z</sub> was extremely disturbed and fluctuated sharply in north and south directions until grasping the maximum value northward to 17.53 nT in the early hours of 20 December. SSC was followed by a prolonged initial phase with dominant northward fluctuation of IMF-B<sub>Z</sub>. Subsequently, solar wind speed sharply increased from 361.2 km/s to 504.7 km/s, value of density elevated to 53.63 n/cc and pressure to 25.68 nPa in the initial phase.

The escalation in density and/or speed of the solar wind signifies the sudden storm commencement (SSC) (Willis, 1964) which is marked as the inception phase of a geomagnetic storm (de Abreu et al., 2014). Sym-H displayed the smooth evolution from the onset of initial phase and attained the highest value of 45 nT on 19 December. Then, IMF B<sub>Z</sub> immediately shifted southwards dropping down to -16.58 nT and the value of Sym-H started to decline at 04:28 UT on 20 December marking the onset of main phase. Attaining the highest negative value of -18.96 nT at 23:26 UT on 20 December, fluctuation of IMF B<sub>Z</sub> lasted for about 33 hours in southward direction. Sym-H attained the supreme negative value of ~-170 nT indicating an intense geomagnetic storm and initiated the recovery phase from 22:53 UT on 20<sup>th</sup> December. There was brisk fluctuation of IMF-B<sub>Z</sub> from 21:11 UT of 21 December to the end of 22 December spotting the terminus of the recovery phase. The turning of IMF-B<sub>Z</sub> from abiding northward configuration to the southward generates a dawn to dusk convection electric fields being active in the main phase and leads to undershielding condition at higher latitudes (Huang et al., 2005; Kikuchi et al., 2008; Ramsingh et al., 2015). Resulting electric field will be westward during nighttime and eastward during daytime. After the prevalence of IMF-B<sub>Z</sub> for a certain time in southward direction, it switches to northward again resulting overshielding condition which is active in the recovery phase (Ramsingh et al., 2015).

The value of solar wind speed returned to its initial value of 396.4 km/s at 08:31 UT on 20 December and remained almost constant till the end of same day. It showed a nature of sparse variation during the recovery phase. The graph of pressure and density almost displayed the analogous pattern in this case as well. The maximal value of pressure amounts to 25.68 nPa at 21:39 UT on 19 December and that of density approaches to 71.92 cm<sup>3</sup> at 8:15 UT on 20 December. The value of both pressure and density splash the fluctuating behavior dropping down to almost zero on 23:27 UT on 20 December but still parades some accession from the edge of 21 December to the mid of 22 December during the recovery phase. Protracted and rapid disparity with several peaks was observed in the graph of AE index which remained quiet before SSC. AE showed the increment twice nearly 764 nT and 872 nT at 16:41 UT and 21:41 UT on 19 December. The following day AE procured the three highest peak values as 1472 nT, 1810 nT and 1946 nT at 05:18 UT, 12:22 UT and 16:13 UT during the main phase and commenced to decline eventually with the onset of recovery phase on 21 December. It portrayed a meager digression twice on 22 December.

This event has got a unique nature in which the storm is characterized as High Intensity Long Duration Continuous Auroral-Electrojet Activity (HILDCAA) caused by Interplanetary Coronal Mass Ejection (ICME) associated with the magnetic cloud resulting huge disturbance in geomagnetic field. HILDCAA events can be literally identified and classified based on AE index. AE index mounted to value of 1472 nT during the onset of main phase and does not tumble below 200 nT continuously for more than 2 hours. Moreover, fluctuation in AE index has lasted for more than 2 days that can be observed during the long-lasting recovery phase till the end of 22 December. These criteria of AE index signify the event as HILDICAA (Tsurutani and Gonzalez, 1987, 2013). The continuous injection of energetic particles into the magnetosphere due to Joule heating at auroral latitude results in long recovery phase during HILDICAA (Aksnes et al., 2004). HILDICAA events associated with Co-Rotating Interaction Region (CIR) is portrayed with the brisk fluctuation in IMF  $B_z$  whereas ICME HILDICAA is accompanied by low amplitude fluctuation of negative IMF  $B_z$  value turning southwards (Tsurutani et al., 2006, Adhikari et al., 2017, Adhikari et al., 2019). As figure interprets the fluctuations in negative values of IMF  $B_z$  for 33 hours in southward direction, it can be concluded that this storm is delineated by HILDICAA events preceded by ICME (Tsurutani and Gonzalez, 1987).

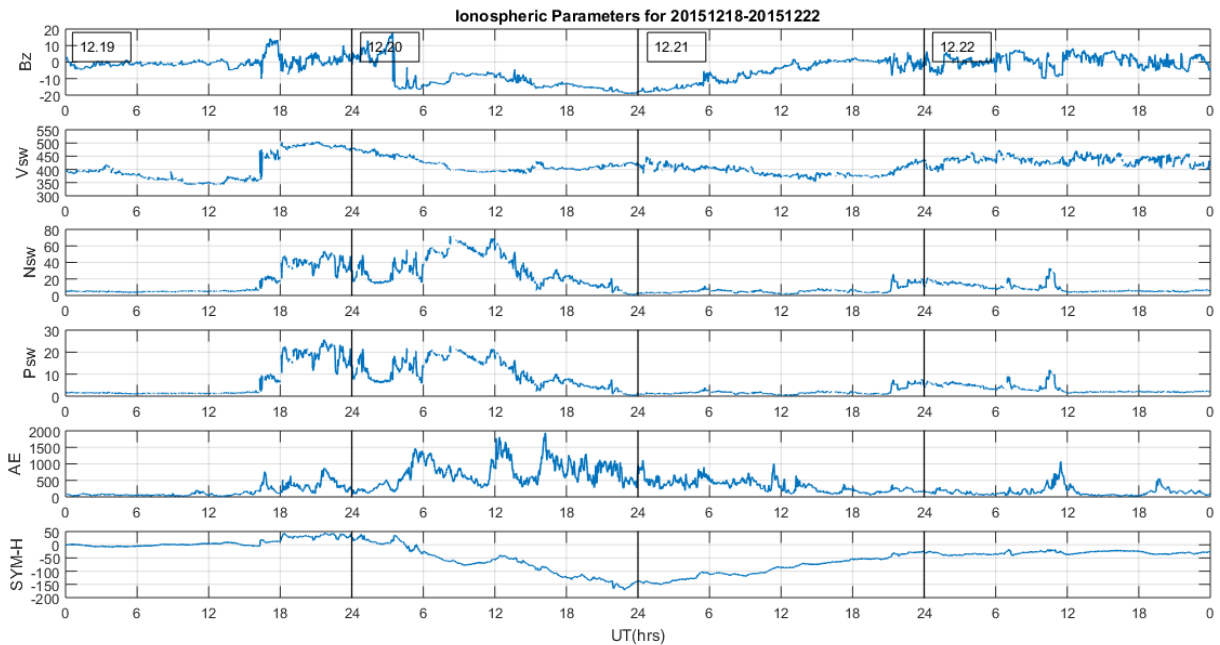


Fig. 12. z-component of interplanetary magnetic field IMF- $B_z$  (nT), solar wind speed  $V_{sw}$  (km/s), solar wind density (cm<sup>3</sup>), solar wind pressure (nPa), auroral electrojet AE index (nT) and symmetrical ring current index Sym-H (nT) for the period 19 December - 22 December 2015 are presented from top to bottom panels

Figure 13 illustrates the fluctuation of VTEC at the previously mentioned stations and mean quiet day over the duration of 19<sup>th</sup> June to 22<sup>nd</sup> December 2015. VTEC is a parameter used to explain the global demeanor of the ionospheric responses to the geomagnetic storm (Jin et al., 2017). Second panel of graph delineates the combined fluctuations of VTEC over iisc, hyde, lck3 stations of India at low latitudes. At the very beginning, all the values are near about a mean quiet day but rapid changes have been analyzed in VTEC with hyde station attaining the highest value of 48.92 at 15:12 LT on 19 December before the initiation of SSC and gradually decreasing after the onset of SSC. VTEC is immensely detected during day time and haltingly diminishing during night time following a similar pattern in next three days. Among the three stations, the graph of lck3 shows the minimal variation of VTEC from the beginning phase till 21 December and an abrupt transition is delineated around 15:36 LT as 54.23 on 22 December exceeding the value of mean quiet day . The largest value is enacted by the station hyde at 15:02 LT as 56.6 on 22 December during the recovery phase. The escalation and decline in VTEC results in the positive and negative ionospheric storms (Fagundes et al., 2016).

Despite incidence of intense geomagnetic storm, no peculiar effect in VTEC concentration is observed. Instead, it displayed a pattern of regular daily variation. The regular daily variation may be due to higher solar wind velocity during day and lesser during night. The apical perturbation on VTEC is spotted in the mid-afternoon and commence to decline afterward. This diminution in VTEC may be the effect of westward polarity of DD (disturbance dynamo) electric field leading to contraction of equatorial ionization anomaly (EIA) (Tsurutani et al., 2004). The rise and fall in the VTEC values fabricated a wave-like VTEC oscillation which firmly disturbed the equatorial ionization anomaly (EIA) during the main and recovery phase (Fagundes et al., 2016).

According to Wang et al., (2010) positive phases are chiefly prevailing aspect in the low- and middle-latitudes during the initial and main phase. Negative phases at midnight arise due to consecutive modification in neutral composition and night-side equatorial wind (Jin et al., 2017). From the inspection of data from the stations like darw, tow2 and mchl of Australia, the maximum VTEC count 58.48 and 48.62 has been displayed by the darw and tow2 around 17:40 LT and 13:26 LT on 20 December whereas mchl show the largest VTEC count as 40.69 on 17:58 LT on 20 December. The VTEC count was maximum on 20 December and subtle on 21 December as compared to other days where all the stations were recorded to have VTEC values more than the mean quiet day. All the three stations of Australia demonstrated drastic change on 21 December in VTEC as a consequence of the geomagnetic storm that might be due to the accumulation of charged particle in ionosphere and magnetosphere. This sharp inconstancy in VTEC value ensued from main phase to recovery phase.

Brazilian stations savo, braz and ufpr showed that savo parades greater disparity at the initial phase of geomagnetic storm on 19 December as compared to other two sites. All three stations show the similar pattern attaining the extreme value at mid-afternoon and continuously dropping afterward during the nighttime. VTEC count was almost equivalent on 20 December and 22 December which was apical among all 4 days. Except 21<sup>st</sup> December all the stations exhibited greater VTEC values than the average quiet day. South African stations as wind, hrao and rbay depict the lowest VTEC deviation compared to other stations attaining highest value during daytime and lowest during nighttime, following the equivalent pattern in other three days. Remarkable alterations weren't observed from the mean quiet day values. Extreme impacts of the storm were detected on 21 December during the recovery phase in all stations of Brazil, Australia and South Africa.

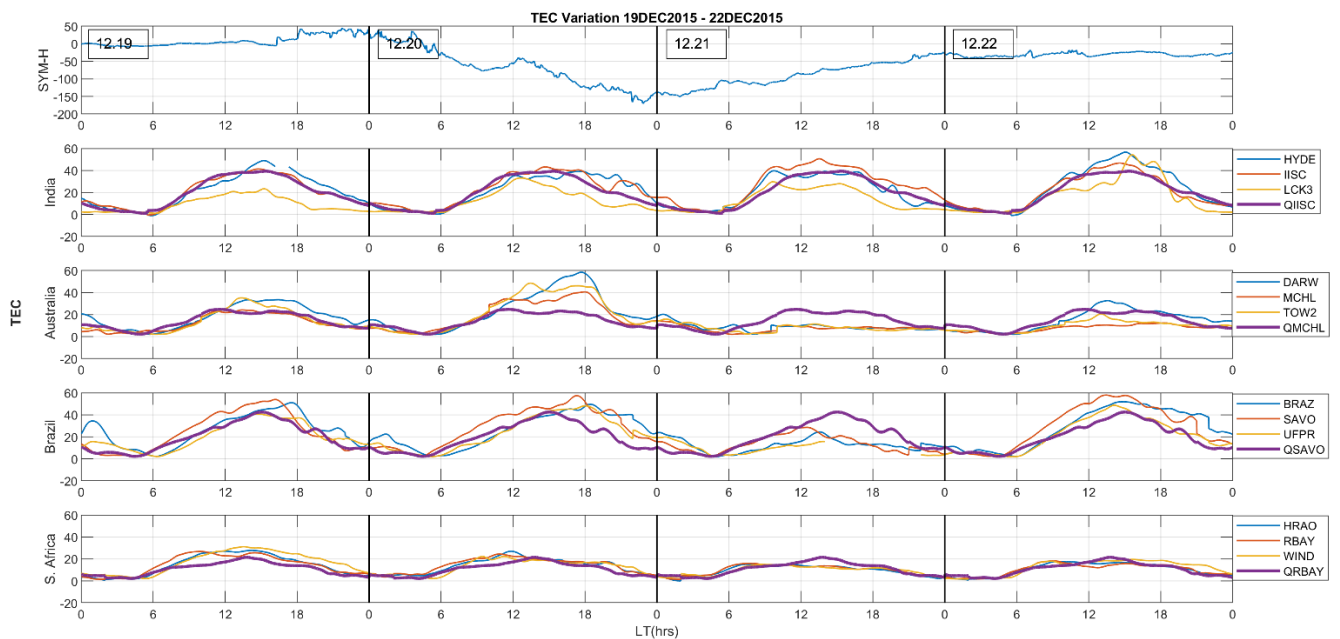


Fig. 13. VTEC variation observed on multiple stations of India (hyde, iisc, lck3), Australia (darw, mchl, tow2) Brazil (braz, savo, ufpr) and South Africa (hrao, rbay, wind) from 19th of December to 22nd of December 2015 at regular intervals of LT are presented from top to bottom panels along with the mean quiet day.

Figures 14 and 15 describe contrast in Total Electron Content (TEC) throughout the globe during the geomagnetic storm of 20<sup>th</sup> and 21<sup>st</sup> December 2015. During the activation of storm at 00:00 UT on 20 December, intensified TEC is observed over Pacific Ocean at the equatorial and low-latitude regions, faint effects over Brazilian sectors whereas minimum effects are noticed in the Indian belts. The mild TEC variation is detected near the Northern Australia at 06:00 UT. At 08:00 UT on 20 December, the highly intensified TEC effects are seen across southern China and near Indonesia including some parts of Australia represented by dark yellow color. de Jesus et al. (2016) has studied the dynamics of the ionosphere and its response during severe

geomagnetic storm and observed exclusively specific features in solar cycle 24 in reference to other solar cycles. Simi et al. (2013) and Huang (2013) observed that acute disruption of global winds (surging towards equator from higher latitudes) and electric fields commenced from magnetosphere-ionosphere interaction cause the severe modification in the equatorial, low-latitude region (de Abreu et al., 2014).

Soon the TEC variations get extended over Indian and African zones at 10:00 UT near equatorial planes. After the fabrication of adverse impacts over African and Indian belts, the enhanced TEC shifts towards westward equatorial region with minimizing effects in the eastern side and abruptly rises near the South Atlantic Ocean showing some effects in the Brazilian zone at 14:00 UT. TEC gets prolonged towards the Pacific Ocean at low latitude with diminishing amount in the Brazilian sector and minimum in the Australian and Indian plates till 20:00 UT. The most extreme TEC is observed on 22:00 UT on 20 December which remained until the early hours of 21 December between  $-30^{\circ}$  to  $30^{\circ}$  latitude across the Pacific Ocean indicated by dark yellow color. The acute value of TEC might have been emerged from the alteration in global winds circulation associated with the procreation of travelling ionospheric disturbances (TIDs) in the auroral regions induced by Joule heating during the main and recovery phase (Fuller-Rowell et al., 1994; Killeen et al., 1984; Fagundes et al., 1995).

Firm innovation in TEC is seen overall in African and Indian sectors from 6:00 UT to 12:00 UT on 21 December with mild effects in Australian and Brazilian sectors. Subsequently, it proceeds along the westward equatorial and low-latitude planes and suddenly magnifies in the African, Brazilian and South Atlantic Ocean including the Pacific Ocean leaving moderate effects in Indian and Australian belts from 14:00 – 18:00 UT on 21 December. The amplification of TEC diverges towards Pacific region and intense TEC is remarked at 22:00 UT near equatorial and South Pacific Ocean on 21 December. Protracted span of positive ionospheric storm observed at equatorial and low-latitude regions is due to TEC variations correlated with equatorward neutral winds and huge wind circulations (de Jesus et al., 2016). The modification of ionospheric dynamics at the equatorial and low-latitudes might be due to the effect of prompt penetration of magnetospheric electric field during the main phase of the storm when the Dst index fluctuated sharply (Basu et al., 2001; Lu et al., 2012).

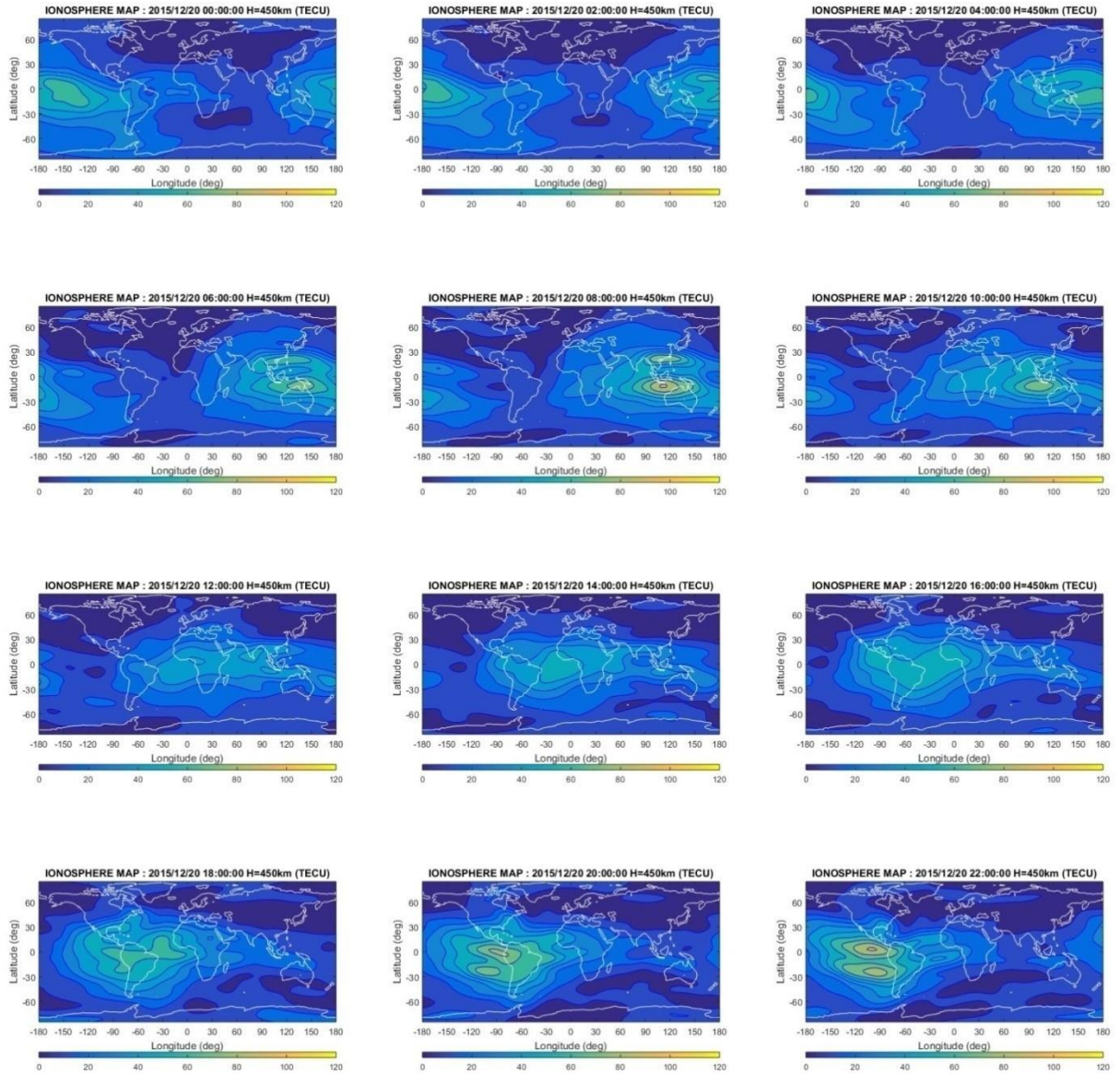


Fig. 14. Global GPS-TEC maps portraying geomagnetically disturbed days of 20th December 2015 at regular interval of 2 hours in UT

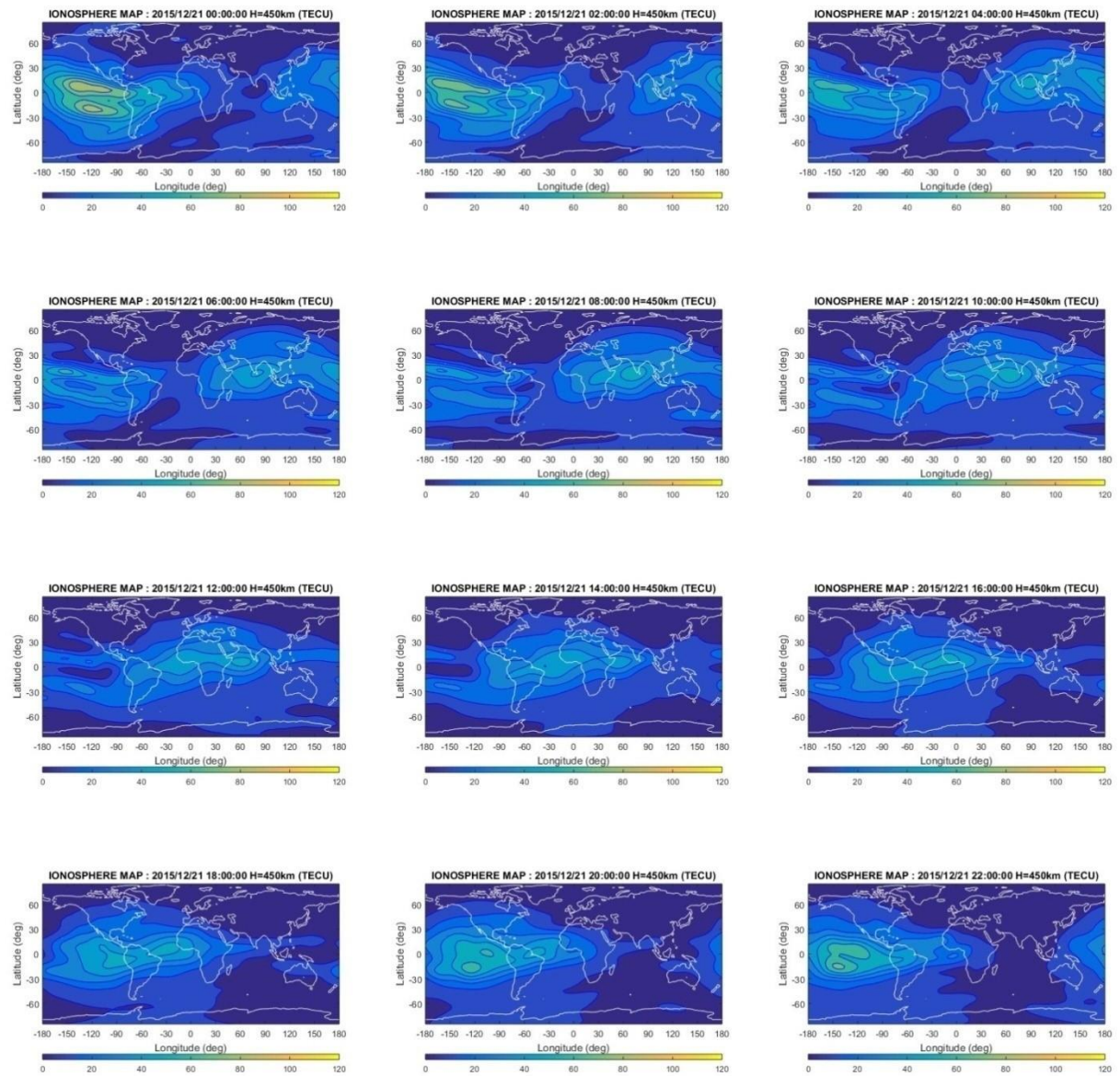
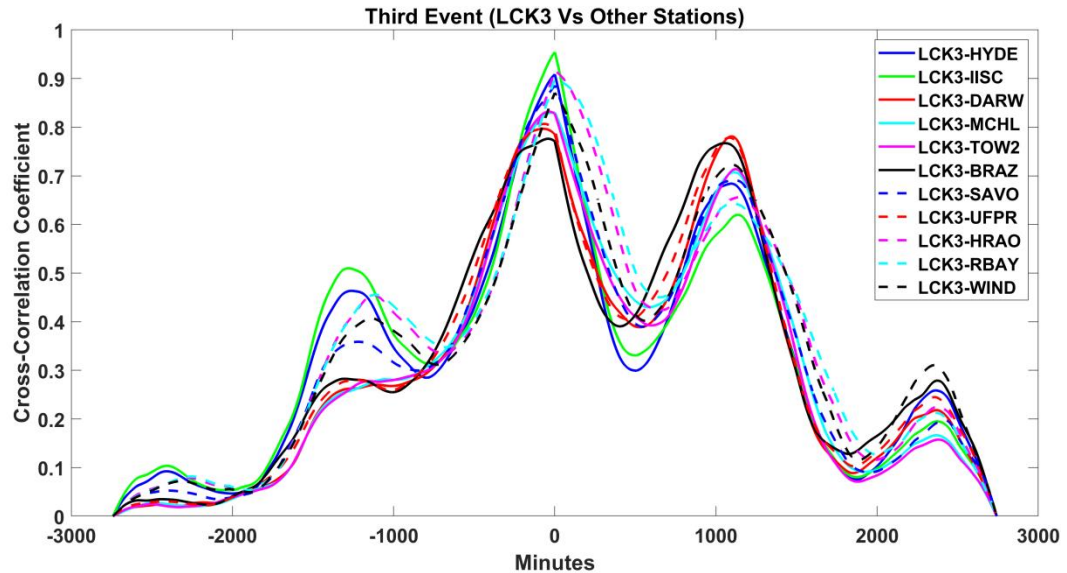


Fig. 15. Global GPS-TEC maps portraying geomagnetically disturbed days of 21st December 2015 at regular interval of 2 hours in UT



**Figure 16.** Cross-correlation of symmetric horizontal component of geomagnetic field (SYM-H) of LCK3 station with other stations, HYDE (solid blue), IISC (solid green), DARW (solid red), MCHL (solid sky blue), TOW2 (solid pink), BRAZ (solid black), SAVO (dotted blue), UFPR (dotted red), HRAO (dotted pink), RBAY (dotted sky blue) and WIND (dotted black) during intense storm caused by ICME occurred on 19-21 December 2015.

Figure 16 illustrates the correlation between *TEC* of LCK3 station and various other stations during the storm preceded by ICME on 19-21 December 2015. The time scale displayed by x-axis runs from -3000 to 3000 min and the cross-correlation coefficient displayed by the y-axis ranges from 0 to 1. This plot shows peculiar nature. More fluctuations can be observed as compared with other two events. Several positive peak value of correlation coefficients can be seen in this plot. LCK3-IISC (solid green) depicts the supreme value of positive correlation coefficient of 0.975 at 0 min in the first peak. Similarly, LCK3-HRAO (dotted pink) and LCK3-HYDE (solid blue) show the highest positive correlation coefficient of 0.908 at time 0 min whereas other stations positively correlates with LCK3 between 0.780 to 0.893 at time interval from -100 to 80 min in the first peak. Furthermore, we can observe the rise in value of correlation coefficient denoting the second peak of 0.791 by LCK3-DARW (solid red) and LCK3-UFPR (dotted red) curves at 1098 min time lead. Other stations also positively correlate with LCK3 at this moment. Moreover, moderate cross correlation is reflected in the third peak by LCK3-IISC pair as 0.509 at -1250 min time lag.

## 5. Conclusion

Studying IMF-Bz, Solar wind parameters ( $V_{sw}$ ,  $N_{sw}$ ,  $P_{sw}$ ) and Geomagnetic indices (AE and SYM-H) helps to analyse the different types of solar activities. In this study, we present and analyze the results using simultaneous VTEC data from 12 GPS-TEC stations over the Indian, Australian, Brazilian and South African regions during three geomagnetic events. The 17th and 18th March of 2015 has been noted best date to observe the heavy geomagnetic storm of solar cycle 24 due to CME. The 17th March storm was followed by a recurrent magnetic storm. Interlinking the parameters with heavy fluctuating TEC in the stations of Brazil and India whereas, S.African and Australian stations showing less fluctuations than others. This phenomenon was marked as Tidal Ionospheric Disturbances(TID), generally initiating at high latitudes and traveling towards equatorial direction. It was found that heavily TEC influenced area were found to be transposing through equatorial plane starting from eastern sectors to the western sectors. Indian Ocean sectors, Atlantic Ocean and South Pacific Ocean were affected followingly. TEC Maps evince that Indian and Brazilian sectors were affected heavily explaining the TID as seen on those areas.

Geomagnetic disturbances examined during June (21st – 23rd ) 2015 reveals the arrival of three IS associated with coronal mass ejections (CME).The June 2015 storm was specified by increased substorm activity. One of the main traits of this storm is significant fluctuations of the IMF Bz during main phase and recovery phase. Among all the stations Braz station of Brazil exhibits highest count of TEC at the main phase but Indian stations recorded more values of TEC than rest of the stations. There were no any significant fluctuations at the starting of the recovery phase. Indian, Australian and S. African stations attain their highest TEC values of the event during the recovery phase. TEC, when observed at Global Ionospheric Maps, prolongs towards lower latitudinal region (30 to -30 degree) through equatorial plane during the event. An Indian region illustrates significant concentration of TEC on the Maps. Mild Intensification over Australian region only during recovery phase is also the significant observation of this event.

The intense geomagnetic storm occurred during 19-22 December in 2015 has got a peculiar result compared to other storms of solar cycle 24. HILDICAA preceded by ICME associated with magnetic cloud is observed even in absence of Alfvénic waves at the descending phase of solar cycle. Generally, other researches depict that HILDCAA events turn up at the maximum phase of solar cycle. But from this event, we can conclude that any types of storm including HILDICAA events can emanate at any phase of solar cycle. Long-lasting fluctuation of IMF BZ for about 33 hours has been inspected in southward direction. Another specific feature illustrated by this event can be discerned from the graph of TEC variation.

Impact of geomagnetic storm on TEC can be perceived in other regions except in Indian sector. Indian sector has shown a pattern of regular daily variation in the graph of TEC. The modification of ionospheric dynamics at the equatorial and low-latitudes might be due to the effect of prompt penetration of magnetospheric electric field during the main phase of the storm when the Dst index fluctuated sharply. On Global Ionospheric Maps, the apical perturbation on VTEC is spotted in the mid-afternoon and commence to decline afterward. This diminution in VTEC may be the effect of westward polarity of DD (disturbance dynamo) electric field leading

to contraction of equatorial ionization anomaly (EIA). Thus, it can be concluded that global ionospheric maps has portrayed the fact that the equatorial and low-latitude regions have been mainly affected by the geomagnetic storms. This phenomenon was marked as Tidal Ionospheric Disturbances (TID), generally initiating at high latitudes and traveling towards equatorial direction. We also checked the cross correlation of *TEC* of LCK3 station and various other stations during the period of high solar and geomagnetic activities; the correlation gradually increased with the near by stations by latitudes in most of the cases which was another intriguing result. Thus this results suggested that the storms were affected globally which is why we believe that variation of *TEC* over various stations of the globe could turn out to be very helpful in predicting solar wind coupling with magnetosphere-ionosphere.

## Acknowledgements:

IMF-Bz, Solar wind parameters ( $V_{sw}$ ,  $N_{sw}$ ,  $P_{sw}$ ) and Geomagnetic indices (AE and SYM-H) data are obtained from the OMNI (<http://omniweb.gsfc.nasa.gov/form>) site. The RINEX Hatanaka compressed observation files extracted from the NASA website (<ftp://cddis.gsfc.nasa.gov/pub/gps/data>). Ionex database derived from NASA site (<ftp://cddis.nasa.gov/pub/gps/products/ionex/>). The conversion of geographical latitude and longitude to magnetic latitude and longitude was processed by World Data Center for Geomagnetism, Kyoto (<http://wdc.kugi.kyoto-u.ac.jp/igrf/gggm/>). The authors would like to acknowledge them.

## References

- Adhikari, B., R. K. Mishra, D. Pandit, B. Bhattarai, N. P. Chapagain (2017), Ionospheric effects of non-storm HILDCAA (High Intensity Long Duration Continuous Auroral Activity), *Journal of Institute of Science and Technology*, 22 (1), 34-40.
- Adhikari, B., S. Dahal, R. K. Mishra, N. Sapkota, N. P. Chapagain, D. N. Chhatakuli, S. Sapkota, S. Adhikari (2019), Analysis of Solar, Interplanetary and geomagnetic parameters during solar cycles 22, 23 and 24, *Russian Journal of Earth Sciences*, 19, ES1003, doi: 10.2205/2018ES000645.
- Aggarwal, M. (2011), TEC variability near northern EIA crest and comparison with IRI model, *Adv. Space Res.*, 48(7), 1221–1231, doi: 10.1016/j.asr.2011.05.037.
- Aksnes, A., J. Stadsnes, G. Lu, N. Østgaard, R. R. Vondrak, D. L. Detrick, T. J. Rosenberg, G. A. Germany, M. Schulz (2004), Effects of energetic electrons on the electrodynamics in the ionosphere., *Ann. Geophys., European Geosciences Union*, 22(2), 475–496, hal-00317232.
- Anderson, D.N. (1973), A theoretical study of the ionospheric F-region equatorial anomaly – I. Theory, *Planet. Space Sci.*, 21(3), 409–419, doi: 10.1016/0032-0633(73)90040-8.
- Astafyeva, E., I. Zakharenkova, and M. Forster (2015), Ionospheric response to the 2015 St. Patrick's Day storm: A global multi-instrumental overview, *J. Geophys. Res. Space Physics*, 120, 9023–9037, doi:10.1002/2015JA021629.
- Astafyeva, E., I. Zakharenkova, J. D. Huba, E. Doornbos, and J. van den IJssel (2017), Global Ionospheric and thermospheric effects of the June 2015 geomagnetic disturbances: Multi-

- instrumental observations and modeling, *Journal of Geophysical Research: Space Physics*, 122(11), 11716–11742, doi: 10.1002/2017JA024174.
- Baker D. N., A. N. Jaynes, S. G. Kanekal, J. C. Foster, P. J. Erickson, J. F. Fennell, J. B. Blake, H. Zhao, X. Li, S. R. Elkington, M. G. Henderson, G. D. Reeves, H. E. Spence, C. A. Kletzing, J. R. Wygan (2016), Highly relativistic radiation belt electron acceleration, transport, and loss: large solar storm events of March and June 2015, *J. Geophys. Res. Space Phys.*, 121(7), 6647–6660, doi: 10.1002/2016JA022502.
- Basu, S., S. Basu, C. E. Valladares, H.-C. Yeh, S.-Y. Su, E. MacKenzie, P.J. Sultan, J. Aarons, F. J. Rich, P. Doherty, K. M. Groves, and T. W. Bullett (2001), Ionospheric effects of major magnetic storms during the International Space Weather Period of September and October 1999: GPS observations, VHF/UHF scintillations, and in situ density structures at middle and equatorial latitudes, *J. Geophys. Res.* 106(A12), 30389–30413, doi: 10.1029/2001JA001116.
- Bilitza, D., B. W. Reinisch (2008), International reference ionosphere 2007: Improvements and new parameter., *Adv. Space Res.*, 42(4), 599–609, doi: 10.1016/j.asr.2007.07.048.
- Blagoveshchenskii, D. V. (2013), Effect of Geomagnetic Storms (Substorms) on the Ionosphere:1, A Review *Geomagnetism and Aeronomy*, 53(3), 275–290, doi: 10.1134/S0016793213030031.
- Blanc M. and A. Richmond (1980), The ionospheric disturbance dynamo, *J. Geophys. Res.*, 85( A4), 1669– 1686, doi: 10.1029/JA085iA04p01669.
- Chapagain, N. P., M. J. Taylor, J. J. Makela, and T. M. Duly (2012), Equatorial plasma bubble zonal velocity using 630.0 nm airglow observations and plasma drift modeling over Ascension Island, *J. Geophys. Res.*, 117, A06316, doi:10.1029/2012 JA 017750.
- Chapagain, N. P., D. J. Fisher, J. W. Meriwether, J. J. Makela, and J. L. Chau (2013), Comparison of Zonal Neutral Winds with Equatorial Plasma Bubble and Plasma Drift Velocities, *J. Geophys. Res. Space Physics*, 118, doi:10.1002/jgra.50238.
- Cherniak I and I. Zakharenkova (2017), New advantages of the combined GPS and GLONASS observations for high-latitude ionospheric irregularities monitoring: case study of June 2015 geomagnetic storm, *Earth, Planets and Space*, 69:66, doi: 10.1186/s40623-017-0652-0.
- Danilov, A. D. (2013), Ionospheric F-region response to geomagnetic disturbances., *Adv. Space Res.*, 52(3), 343–366, doi:10.1016/j.asr.2013.04.019.
- de Abreu, A. J., P. R. Fagundes, Y. Sahai, R. de Jesus, J. A. Bittencourt, C. Brunini, M. Gende, V. G. Pillat, W. L. C. Lima, J. R. Abalde, A. A. Pimenta (2010), Hemispheric asymmetries in the ionospheric response observed in the American sector during an intense geomagnetic storm, *J. Geophys. Res.*, 115(A12), A12312, doi: 10.1029/2010JA015661.
- de Abreu, A. J., Y. Sahai, P. R. Fagundes, F. Becker-Guedes, R. de Jesus, F. L. Guarnieri, V. G. Pillat (2010a), Response of the ionospheric F-region in the Brazilian sector during the super geomagnetic storm in April 2000 observed by GPS, *Adv. Space Res.* 45(11), 1322-1329, doi: 10.1016/j.asr.2010.02.003.
- de Abreu A. J., P.R. Fagundes, M. Gende, O. S. Bolaji, R. de Jesus, C. Brunini (2014), Investigation of ionospheric response to two moderate geomagnetic storms using GPS–TEC measurements in the South American and African sectors during the ascending phase of solar cycle 24, *Advances in Space Research* 53(9), 1313–1328, doi: 10.1016/j.asr.2014.02.011.
- de Jesus, R., P.R. Fagundes, A. Coster, O. S. Bolaji, J. H. A. Sobral, I.S. Batista, A. J. de Abreu, K. Venkatesh, M. Gende, J. R. Abalde, and S. G. Sumod (2016), Effects of the intense geomagnetic storm of September-October 2012 on the equatorial, low- and mid-latitude F region in the American and African sector during the unusual 24<sup>th</sup> solar cycle, *Journal of Atmospheric and Solar-Terrestrial Physics*, 138, 93-105, doi: 10.1016/j.jastp.2015.12.015.
- Dmitriev, A. V., A. V. Suvorova, M. V. Klimenko, V. V. Klimenko, K. G. Ratovsky, R. A. Rakhmatulin, and V. A. Parkhomov (2017), Predictable and unpredictable ionospheric disturbances during St. Patrick's Day magnetic storms of 2013 and 2015 and on 8–9 March 2008, *J. Geophys. Res. Space Physics*, 122(2), 2398–2423, doi:10.1002/2016JA023260.

- Duly, T. M., N. P. Chapagain, and J. J. Makela (2013), Climatology of nighttime medium-scale traveling ionospheric disturbances (MSTIDs) in the Central Pacific and South American sectors, *Ann. Geophys.* 31(12), 2229-2237, doi: 10.5194/angeo-31-2229-2013.
- Ezquer, R. G., N. O. de Adler, S. M., Radicella, M. M. Gonzalez, J. R. Manzano (1992), Total electron content obtained from ionogram data alone., *Radio Sci.*, 27(3), 429–434, doi: 10.1029/91RS02634.
- Ezquer, R. G., N. O. de Adler, T. Heredia (1994), Predicted and measured total electron content at both peaks of the equatorial anomaly, *Radio Sci.*, 29, 831-838, doi: 10.1029/94RS00614.
- Fagundes, P. R., A. L. Aruliah, D. Rees, J. A. Bittencourt, (1995), Gravity wave generation and propagation during geomagnetic storms over Kiruna (67.8°N, 20.4°E), *Ann. Geophys.* 13 (4), 358–366, doi: 10.1007/s00585-995-0358-7.
- Fagundes, P. R., F. A. Cardoso, B. G. Fejer, K. Venkatesh, B. A. G. Ribeiro, and V. G. Pillat (2016), Positive and negative GPS-TEC ionospheric storm effects during the extreme space weather event of March 2015 over the Brazilian sector, *J. Geophys. Res. Space Physics*, 121, 5613–5625, doi:10.1002/2015JA022214.
- Fuller-Rowell, T. J., M. V. Codrescu, R. J. Moffet, S. Quegan (1994), Response of the thermosphere and ionosphere to geomagnetic storms, *J. Geophys. Res.*, 99 (A3), 3893–3914, doi: 10.1029/93JA02015.
- Gonzalez, W. D., J. A. Josely, Y. Kamide, H. W. Korehl, G. Rostoker, B. T. Tsurutani, and V. M. Vasylianas (1994), What is a geomagnetic storm?, *J. Geophys. Res.*, 99(A4), 5771–5792, doi:10.1029/93JA02867.
- Gulyaeva, T. L., X. Huang, B.W. Reinisch (2002), Plasmaspheric extension of topside electron density profiles., *Adv. Space Res.*, 29 (6), 825–831, doi: 10.1016/S0273-1177(02)00038-8.
- Hartman, G. K., R. Leitinger (1984), Range errors due to ionospheric and tropospheric effects for signals frequencies above 100 MHz., *Bull. Geod.*, 58(2), 109–136.
- Huang, C. S., J. C. Foster, L. P. Goncharenko, P. J. Erickson, W. Rideout, and A. J. Coster (2005), A strong positive phase of ionospheric storms observed by the Millstone Hill incoherent scatter radar and global GPS network., *J. Geophys. Res.*, 110(A6), A06303, doi: 10.1029/2004JA010865.
- Huang, C.M. (2013), Disturbance dynamo electric fields in response to geomagnetic storms occurring at different universal times., *J. Geophys. Res.*, 118(1), 496–501, doi: 10.1029/2012JA018118.
- Jin S., R. Jin, H. Kutoglu (2017), Positive and negative ionospheric responses to the March 2015 geomagnetic storm from BDS observations., *J Geod.* 91(6), 613-626, doi: 10.1007/s00190-0-016-0988-4.
- Kikuchi, T., H. Lühr, T. Kitamura, O. Saka, and K. Schlegel (1996), Direct penetration of the polar electric field to the equator during a DP 2 event as detected by the auroral and equatorial magnetometer chains and the EISCAT radar, *J. Geophys. Res.*, 101(A8), 17161–17174, doi:10.1029/96JA01299.
- Kikuchi, T., H. Lühr, K. Schlegel, H. Tachihara, M. Shinohara, and T.-I. Kitamura (2000), Penetration of auroral electric fields to the equator during a sub storm, *J. Geophys. Res.*, 105(A10), 23251–23261, doi: 10.1029/2000JA900016.
- Kikuchi, T., K. K. Hashimoto, and K. Nazoki (2008), Penetration of magnetospheric electric fields to the equator during a geomagnetic storm, *J. Geophys. Res.*, 113(A6), A06214, doi: 10.1029/2007JA012628.
- Killeen, T. L., P. B. Hays, G. R. Carignan, R. A. Heelis, W. B. Hanson, N. W. Spencer, L. H. Brace (1984), Ion-neutral coupling in the high-latitude *F* region: Evaluation of ion heating terms from Dynamics Explorer 2, *J. Geophys. Res.*, 89( A9), 7495–7508, doi:10.1029/JA089iA09p07495.
- Lima, W. L. C., F. Becker-Guedes, Y. Sahai, P. R. Fagundes, J. R. Abalde, G. Crowley, and J. A. Bittencourt (2004), Response of the equatorial and low-latitude ionosphere during the space weather events of April 2002, *Ann. Geophys.*, 22(9), 3211–3219, doi:10.5194/angeo-22-3211-2004.

- Liu, G., H. Shen (2017), A severe negative response of ionosphere to the intense geomagnetic storm of 17 March 2015 observed at middle and low latitude stations in China zone, *Advances in Space Research*, 59(9), 2301-2312, doi: 10.1016/j.asr.2017.02.021.
- Liu, J., W. Wang, A. Burns, X. Yue, S. Zhang, Y. Zhang, and C. Huang (2016), Profiles of ionospheric storm-enhanced density during the 17 March 2015 great storm, *J. Geophys. Res. Space Physics*, 121(1), 727-744, doi:10.1002/2015JA021832.
- Liu, Y. D., H. Hu, R. Wang, Z. Yang, B. Zhu, Y. A. Liu, J. G. Luhmann, and J. D. Richardson (2015) Plasma and magnetic field characteristics of solar coronal mass ejections in relation to geomagnetic storm intensity and variability, *The Astrophysical Journal Letters*, 809:L34, doi:10.1088/2041-8205/809/2/L34.
- Lu, G., L. Goncharenko, M.J. Nicolls, A. Maute, A. Coster, L. J. Paxton (2012), Ionospheric and thermospheric variations associated with prompt penetration electric field., *J. Geophys. Res.*, 117(A8), A08312, doi:10.1029/2012JA017769.
- Materassi M., C. N. Mitchell, P. S. J. Spencer (2003), Ionospheric imaging of the northern crest of the Equatorial Anomaly, *Journal of Atmospheric and Solar-Terrestrial Physics*, 65, 1393-1400, doi:10.1016/j.jastp.2003.06.001.
- Mendillo, M. (2006), Storms in the ionosphere: Patterns and processes for total electron content, *Rev. Geophys.*, 44(4), RG4001, doi:10.1029/2005RG000193.
- Nava, B., J. Rodríguez-Zuluaga, K. Alazo-Cuartas, A. Kashcheyev, Y. Migoya-Oru , S. M. Radicella, C. Amory-Mazaudier, and R. Fleury (2016), Middle- and low-latitude ionosphere response to 2015 St. Patrick's Day geomagnetic storm, *J. Geophys. Res. Space Physics*, 121(4), 3421–3438, doi:10.1002/2015JA022299.
- Nayak, C., L.-C. Tsai, S.-Y. Su, I. A. Galkin, A. T. K. Tan, E. Nofri, and P. Jamjareegulgarn (2016), Peculiar features of the low-latitude and mid latitude ionospheric response to the St. Patrick's Day geomagnetic storm of 17 March 2015, *J. Geophys. Res. Space Physics*, 121(8), 7941–7960, doi:10.1002/2016JA022489.
- Nishida, A. (1968), Geomagnetic D<sub>p</sub>2 fluctuations and associated magnetospheric phenomena, *J. Geophys. Res.*, 73(5), 1795–1803, doi:10.1029/JA073i005p01795.
- Oryema B, E. Jurua, F. M. Dujanga and N. Ssebiyonga (2015), Investigation of TEC variations over the magnetic equatorial and equatorial anomaly regions of the African sector, *Advances in Space Research* 56(9), 1939–1950, doi: 10.1016/j.asr.2015.05.037.
- Prolss, M. J. (1978), Travelling atmospheric disturbances as a possible explanation for daytime positive storm effects of moderate duration at middle latitudes., *J. Atmos. Terr. Phys.*, 40(12), 1351–1354, doi:10.1016/0021-9169(78)90088-0.
- Prolss, G. (1995), Ionospheric F-region storms, in *Handbook of Atmospheric Electrodynamics*, vol. 2, edited by H. Volland., pp. 195–248, CRC Press, Boca Raton, Fla.
- Ramsingh, S. Sripathi, S. Sreekumar, S. Banola, K. Emperumal, P. Tiwari, and B. S. Kumar (2015), Low-latitude ionosphere response to super geomagnetic storm of 17/18 March 2015: Results from a chain of groundbased observations over Indian sector., *J. Geophys. Res., Space Physics*, 120(12), 10864–10882, doi:10.1002/2015JA021509.
- Rawer, K., S. Ramakrishnan, D. Bilitza (1978), *International Reference Ionosphere 1978*, International Union of Radio Science, URSI Special Report, 1–75. Bruxelles, Belgium.
- Richardson I.G., and H.V. Cane (2012), Solar wind drivers of geomagnetic storms during more than four solar cycles. *J. Space Weather Space Clim.* 2, A01. doi:10.1051/swsc/2012001.
- Sastri, J. H., N. Jyoti, V. V. Somayajulu, H. Chandra, and C. V. Devasia (2000), Ionospheric storm of early November 1993 in the Indian equatorial region, *J. Geophys. Res.*, 105(A8), 18443–18455 doi:10.1029/1999JA000372.
- Scida, L. A., R. G. Ezquer, M. A. Cabrera, C. Jadur, A. M. Sfer (2016), Tucuman ionospheric model (TIM): Initial results for STEC predictions., *Adv. Space Res.*, 58(6), 821–834, doi: 10.1016/j.asr.2016.05.005.

- Seemala, G.K., Valladares, C.E. (2011), Statistics of total electron content depletions observed over the Southern American continent for the year 2008, *Radio Sci.* 46(5), RS5019, doi: 10.1029/2011RS004722.
- Simi, K.G., G. Manju, M. K. M. Haridas, S. R. P. Nayar, T. K. Pant, and S. Alex (2013), Ionospheric response to a geomagnetic storm during November 8–10, 2004., *Earth Planets Space* 65(4), 343–350, doi: 10.5047/eps.2012.09.005.
- Takashi M., M. A. Guanyi, and N. Maho (2009), Ionospheric storm and variation of total electron content, *Journal of the National Institute of Information and Communication Technology*, Vol. 56 Nos 1-4.
- Thomas, E. G., J. B. H. Baker, J. M. Ruohoniemi, A. J. Coster, and S. R. Zhang (2016), The geomagnetic storm time response of GPS total electron content in the North American sector, *J. Geophys. Res. Space Physics*, 121, 1744–1759, doi:10.1002/2015JA022182.
- Tsurutani B. T. and W. D. Gonzalez (1987), The cause of high-intensity long-duration continuous AE activity (HILDCAAs): Interplanetary Alfvén wave trains. *Planet Space Sci* 35(4), 405–412, doi: 10.1016/0032-0633(87)90097-3.
- Tsurutani, B., et al. (2004), Global dayside ionospheric uplift and enhancement associated with interplanetary electric fields, *J. Geophys. Res.*, 109(A8), A08302, doi:10.1029/2003JA010342.
- Tsurutani B. T. et al. (2006), Corotating solar wind streams and recurrent geomagnetic activity: a review. *J. Geophys. Res.*, 111(A7), A07S01, doi:10.1029/2005JA011273.
- Tsurutani BT and W. D. Gonzalez (2013), The Interplanetary Causes of Magnetic Storms: A Review, In *Magnetic Storms* (eds B. T. Tsurutani, W. D. Gonzalez, Y. Kamide and J. K. Arballo), doi: 10.1029/GM098p0077.
- Verkhoglyadova, O. P., B. T. Tsurutani, A. J. Mannucci, M. G. Mlynczak, L. A. Hunt, L. J. Paxton, and A. Komjathy (2016), Solar wind driving of ionosphere-thermosphere responses in three storms near St. Patrick's Day in 2012, 2013, and 2015, *J. Geophys. Res. Space Physics*, 121(9), 8900–8923, doi: 10.1002/2016JA022883.
- Wang W, J. Lei, A. G. Burns, S. C. Solomon, M. Wiltberger, J. Xu, A. Coster (2010), Ionospheric response to the initial phase of geomagnetic storms: Common features, *J Geophys Res*, 115(A7), A07321, doi:10.1029/2009JA014461.
- Willis, D.M. (1964), The sudden commencement and first phase of a geomagnetic storm, *J. Atmos. Terr. Phys.* 26(5), 581–602, doi: 10.1016/0021-9169(64)90189-8.